Commisioning of the Cooling System for the Bergen Proton Computed Tomography Digital Tracking Calorimeter

By Jakub Bieniek

Supervised by:

Dieter Rudolph Christian Röhrich and Max Philip Rauch

A Master's Thesis in Medicinal Physics

at The Department of Physics and Technology

at The Faculty of Mathematics and Natural Sciences

of University of Bergen

May 2023

Abstract

Particle therapy is a growing field in medicine and medical physics. Compared to standard radiotherapy, it promises treatment with less direct and indirect side-effects to healthy tissues. However, a large issue exists with treatment imprecisions stemming from usage of standard CT for particle treatment planning. As such, building a machine capable of particle CT is extremely desirable. One such prototype developed by the Bergen pCT collaboration is currently in late stages of assembly.

The cooling system of this prototype will be the focus of this thesis. A description of its components and how they work together will be given, both on the hardware and the software level. On the software end, a description will be given of how data from cooling system sensors end up as readable information for the user. Each step in this process will be described, from sensor readout to data retrieval by I/O modules, to software data processing, ending in database storage and front-end parameter display. For the hardware, various properties will be investigated; with sensors and their properties first, including calibrations, limitations and issues. Then a description of thermal properties will be given, with a walkthrough of where the temperatures were measured and why they were measured at those spots. The theoretical and practical calculation of energy supplied and removed will be considered and discussed. The results of all of this will be a working cooling system, with a monitoring setup, which will then be tested to see if it meets our expectations.

The results from various tests on the pCT prototype mock-up show promising results for the tracker and the calorimeter performance, with stable and mostly linear responses to changes in assorted system parameters, like pressure, flow rate or power delivered.

In conclusion, it is expected that many of the results can be used directly to assert the final prototype cooling system performance and temperatures at both the tracker and the calorimeter.

Acknowledgements

I would like to extend my deep gratitude towards everyone who helped and supported me during these two years. My supervisors Dieter Röhrich and Max Rauch, for their guidance and for giving me the opportunity of working with this project. Ton van den Brink, for going above and beyond in helping me understand the Bergen pCT DTC prototype and answering any questions I had related to it. The software meeting group, herein Matthias Richter and Håvard Helstrup, which quickly ended up being a support group for us master students working with this project at UiB. Tea Bodova, a PhD candidate who somehow always found time to help me tinker with the prototype mock-up. Finally, my father Miroslaw, whose support allowed me to go so far in my studies.

Acronyms

AI	Analog Input
ALICE - ITS	A Large Ion Collider Experiment - Inner Tracking System
ALPIDE	ALice PIxel DEtector
CS	Cooling System
DI	Digital Input
DO	Digital Output
DTC	Digital Tracking Calorimeter
MAPS	Monolithic Active Pixel Sensor
PWM	Pulse Width Modulation
RD	Radiodensity
RSP	Relative Stopping Power
RTD	Resistance Temperature Detector

Contents

List of Figures

List of Tables

1 Introduction

Every year, the global number of cancer cases steadily increases [4]. It is a disease which claims millions of lives yearly, and negatively affects many more. Cancer is in many cases preventable and treatable, given early detection. There are many tools in doctors' hands to aid patients with cancer. The three main ones being surgery, chemotherapy and radiation therapy. In recent years a more sophisticated form of radiation therapy, particle therapy, is gathering more and more interest all over the world, as it promises intense treatment of cancer while minimizing damage to healthy tissues. Currently, most particle therapy facilities operate with protons, with some operating with heavier ions like carbon-ions. Many countries already operate these facilities, and Norway is to be one of these countries, with its two proton therapy centers to be finished and operational in 2024 [5].

In addition to treatment facilities, the Bergen pCT Collaboration [6] is currently in its final stage of assembling a proton computed tomography device, capable of 3D image reconstruction of the human body using energetic protons. This device is a hope for making particle therapy even more precise.

1.1 Radiation Therapy and Particle Therapy

Radiation therapy is a common name for all medical treatments involving usage of ionizing radiation. The most known type, called radiotherapy, uses photons in x-ray energy range to irradiate tissue, causing DNA damage through ionization of atoms directly or indirectly by ionization of water creating free radicals [7].

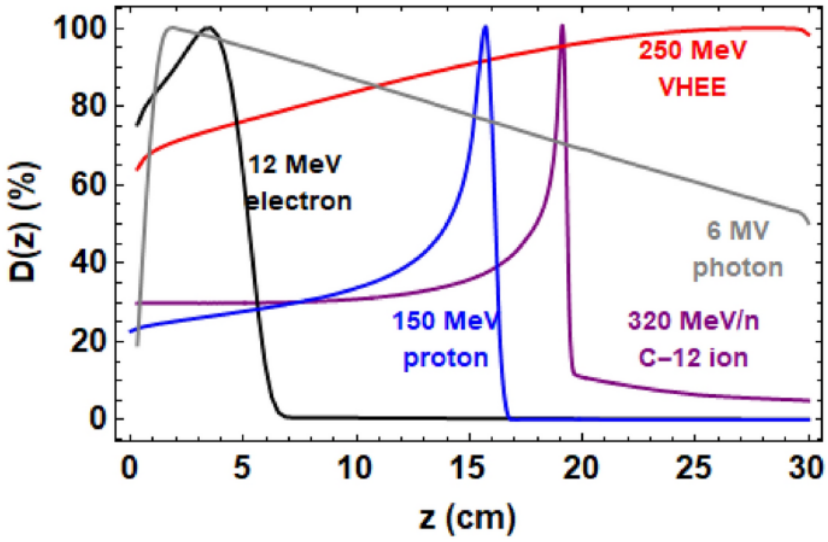

Figure 1: Energy loss curves of various particles at various energies, presenting dose deposited with respect to depth in medium [1].

A photon beam loses energy through attenuation, meaning the radiation dose will always be highest at the entrance, gradually decrease with depth and be non-zero at the exit, exemplified in figure 1. As a result, a significant portion of beam energy is released to healthy tissue surrounding a tumor. The severity of side effects is directly proportional to dose received. Non-stochastic/deterministic effects get more intense, however, more importantly, the probability of stochastic/non-deterministic effects, like radiation-induced malignancies, rises with increased dose. Radiotherapy is therefore problematic in cases where there is low tolerance for collateral damage, like head and neck, and for hypoxic tumors where free radicals are less effective due to lack of oxygen [8].

An alternative approach to radiotherapy is particle therapy. Particle therapy uses energetic beams of protons, neutrons, electrons or other, heavier ions for treatment. For comparison, the typical energy ranges for treatment are 6-20 MeV for photons [9] and 70-250 MeV for protons [10], a significant step-up in energy. Aforementioned particles, excluding electrons which are a special case, look similar to proton energy loss in figure 1. They have a, comparatively to photons, low entrance dose; as well as an exit dose which is usually negligible with some minor secondary ionizations. Depending on the initial energy of the beam and the medium it travels through, the particles will come

to a sudden stop over a small distance causing large amounts of energy to be released within a short depth. This behaviour is seen in figure 1 as a very sharp peak, called a Bragg peak [11]. Bragg peaks are the cornerstone of particle therapy, as they allow in theory for precise deposition of large amounts of energy in a particular volume. For treatment this promises two things: a considerably lower dose to healthy tissue in the path of the beam, as well as a precise dose deposition inside a tumor.

1.2 Proton Computed Tomography

Both radiotherapy and particle therapy require knowledge about what tissues the beam will be passing through on its way to the target to correctly choose the beam energy. A photon beam is attenuated as it travels through tissue, losing its intensity in the process. In order to correctly predict the energy-loss per unit length of the beam, the radiodensity (RD) of each voxel must be known. For radiotherapy, the radiodensity is obtained from a X-Ray Computed Tomography (CT) scan, which conveniently uses photons for imaging.

An analog to materials' RD for photons is materials' stopping power (SP) for massive particles. In particle therapy, instead of SP, we use a quantity called relative stopping power (RSP) instead, which relates a materials' SP relative to that of water [12]. From the value of RSP we can extract the expected range and Bragg peak position of protons. However, currently there is no pCT scanner in clinical use, so existing particle treatment facilities calculate RSP from radiodensity information obtained from standard CT. This conversion is a complex process requiring many approximations and assumptions, as well as knowledge of many different factors at play and quality of algorithms used. Another issue is that this uncertainty, of up to 5% [13], comes on top of standard CT accuracy. Scanning using particles allows us to ignore RD to RSP conversion, meaning that theoretically the overall accuracy of RSP information should be more detailed and precise.

1.3 The Aim of This Work

This work aims to test various aspects of the cooling system designed for the Bergen proton Computed Tomography Digital Tracking Calorimeter (pCT DTC) prototype by

emulating the heat produced as in its finished state. Given the current status of this machine, missing the heat generating sensors, a mock-up using heating elements was constructed in order to emulate them. While this emulation of sensors in the tracker works well, in the calorimeter it doesn't provide proper heat distribution. However, it still provides energy necessary to assess the performance of the cooling system. Performance, as well as various other aspects of the cooling system of the DTC, will be evaluated via assorted set of tests on its mock-up. From the results, a prediction for performance of the finalized cooling system will be given. The list of tests consists of the following:

- Temperature measurement at various power levels to the heating elements
- Temperature measurement at various performance levels of the cooling system
- Thermal stabilization time
- Change in coolant temperature, which allows calculation of energy removed

But first and foremost, as of 2022, the cooling system is unfinished, as it's currently only an aluminium chassis with a water loop and disconnected pressure sensors. Thus requiring a mix of new hardware and software before it can be tested. On the hardware side, the missing pieces are all the services, readout input/output (I/O) devices and sensors. There is no software, so it will be implemented from the ground up into an all-in-one package capable of receiving data from the I/Os, process it and store it in a database with a live display.

2 Bergen Proton Computed Tomography Digital Tracking Calorimeter

The Bergen pCT DTC prototype is currently under construction by the Bergen pCT Collaboration. As the name suggests, it is a digital device tracking both direction of incoming protons, as well as their energy. It is made up of a three main parts;

- A 43 sensor layer DTC; herein two front layers serve as the tracker, tracking the direction of protons allowing identification in the remaining 41 layers, which serve as the calorimeter, tracking particle penetration depth and thus their total energy which remained after passing through the scanned object.
- Services; power boards supplying and distributing power to the DTC, transition cards transferring particle data out to data acquisition boards (DAQ).
- A two-part cooling system consisting of a water cooling and air cooling, together with sensors constantly measuring cooling systems state.

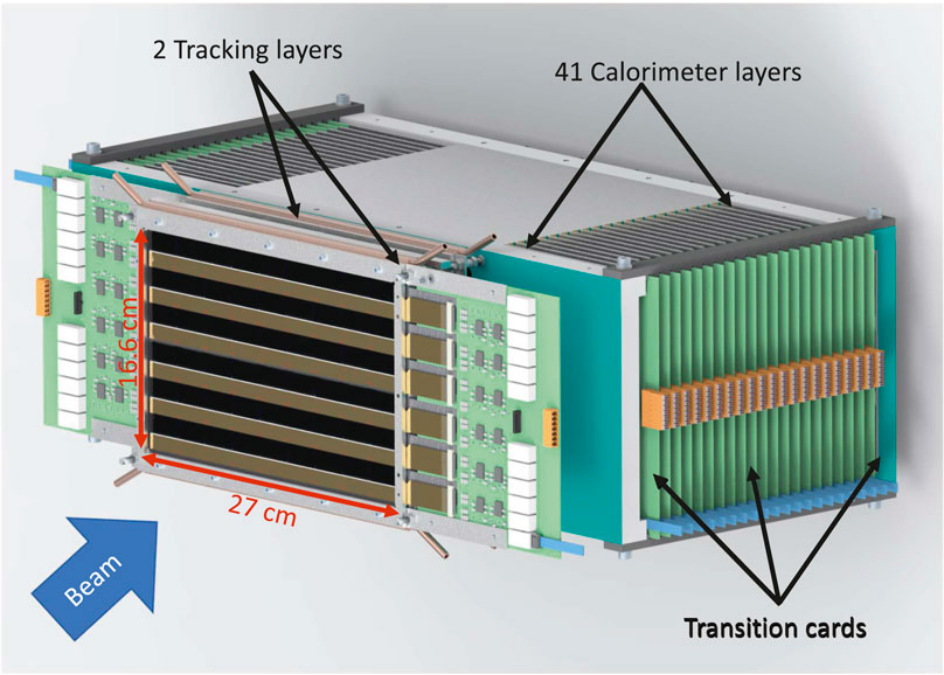

Figure 2: General structure of the Bergen pCT DTC [2].

2.1 Design

This chapter describes the general build of the Bergen pCT DTC and its cooling system. It describes all the parts, what their purpose is and how they all fit together, while also providing pointers on the software end.

2.2 System Parts of the Digital Tracking Calorimeter

2.2.1 ALPIDE Sensors

The sensors of choice for the DTC are the ALPIDE sensors. They were developed as an upgrade for the ALICE Inner Tracking System (ITS) upgrade [14] at European Organization for Nuclear Research (CERN). ALPIDE sensors are 1.5 $cm \times 3$ cm large monolithic active pixel sensors (MAPS). These sensors boast a high spatial resolution of 512×1024 pixels together with good temporal resolution with a peaking time of 2 μs. The other major advantage is the low power density of < 40 mW/cm^2 and a calculated power consumption of 202 mW [2], together with a hit or no-hit readout, with a range of customizable in circuit settings, allowing removal of large swaths of unnecessary or noisy data before it is sent out for processing or storage.

2.2.2 ALPIDE Sensor Layers

ALPIDE sensors are mounted in line, in groups of nine on a flex cable, this is called a *string*. Three such *strings* are then glued onto a 100 $mm \times 290$ $mm \times 1$ mm aluminium carrier, known as a *slab*. *Slabs* are $> 99\%$ pure aluminium [2], with heat conductivity of 220 W/mK. *Slabs* are separated into a top and bottom slab, together making a half-layer in the DTC. In a half-layer, only half of the layer is covered in ALPIDE, with the rest being flex cables. As such, in order to make one layer, two half-layers with alternating ALPIDE *strings* in relation to each other are stacked so that ALPIDEs are on the inside, with a 2 mm gap between them. This layout is consistent between the calorimeter and the tracker, with some major differences in layer material and absorber thickness.

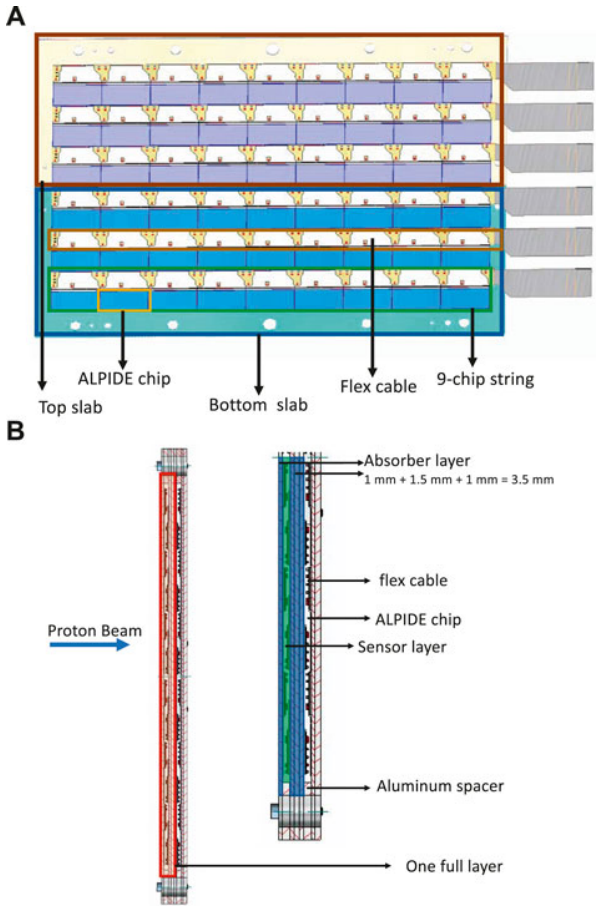

Figure 3: (A) Half-layer layout, (B) Schematic side-view of two layers [2].

Calorimeter layers will consist of 100 $mm \times 290\ mm \times 1\ mm$ aluminium *slabs* screwed to a 200 $mm \times 290\ mm \times 1.5\ mm$ aluminium absorber plate to ensure vertical alignment of the two half-layers, see figure 2A. This gives a total thickness of aluminium in each layer to be 3.5 mm, and the total layer thickness 5.5 mm given the 2 mm air gap, as seen in figure 2B. There will be a total of 41 such layers in the calorimeter, enough to stop a 230 MeV proton beam.

Tracker layers require reduction in particle energy absorption in order to minimize energy losses in those layers. For this reason, six ALPIDE *strings* will be mounted on 200 $mm \times 290\ mm \times 0.2\ mm$ carbon-epoxy(C-E) sheets, serving as a half-layer instead of two aluminium *slabs* with three *strings* each, similarly to 2A. C-E sheets have similar heat conductivity as aluminium of equal dimensions and will be the only thing supporting the ALPIDEs, see[15][16] for more detail on this material. Half-layers

are then mounted in a aluminium frame for rigidity. The total thickness of C-E sheets will be 0.4 mm, with an air gap of 2 mm, giving a total thickness of 2.4 mm per layer. There will be a total of two such layers in the tracker, spaced 50 mm apart [17].

2.2.3 The Transition Cards

All ALPIDE *strings* are connected to a transition card, see figure 2. Transition cards serve as the mediator between the ALPIDE sensors and a connected device receiving data, like a DAQ. All the particle data that the tracker and the calorimeter gather, which would be all the pixel that detected a hit, is sent through the transition card for processing into path and energy reconstruction.

2.3 System Parts of the Cooling System

The physical part of the DTCs cooling system is made up of two main components. These components are the solid metal chassis and the cooling system, consisting of water and air cooling.

2.3.1 The Chassis

The aluminium chassis is the body of the calorimeter. All the calorimeter sensors, cooling loops and ALPIDEs are mounted to it. On top and the bottom of the calorimeter layers are two cooling plates, consisting of aluminium with inserted copper pipes. Tracker layers are mounted to the chassis on a copper frame and are separately cooled. In addition, an extra aluminium frame is mounted to the chassis and holds on to air cooling fans. This was done in order to reduce the amount of vibrations caused by the spinning fans.

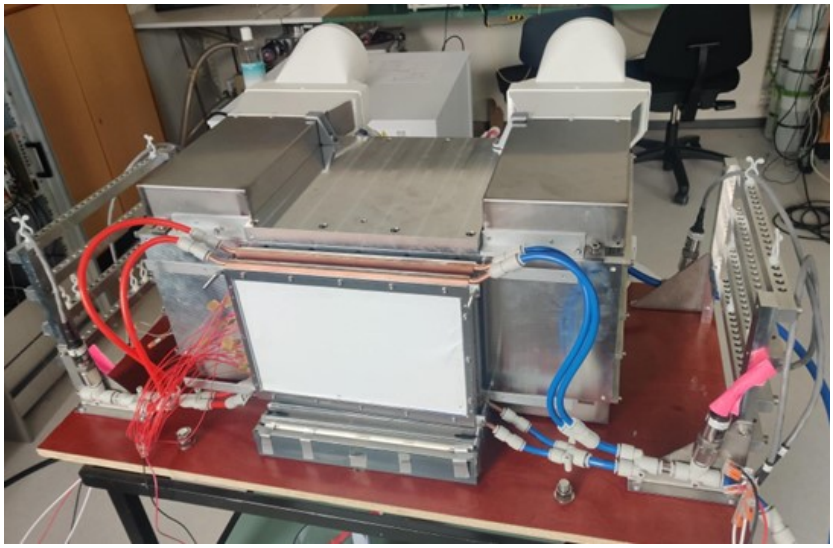

Figure 4: Early photo of the DTC. Two tracker layers are in the front, with the calorimeter chassis behind it and to the sides, with the top cooling plate visible right above the tracker.

2.3.2 The Cooling

The cooling is responsible for keeping the ALPIDEs and transition cards below a specified temperature. Keeping stable temperatures by removing excess heat is a high priority, as ALPIDE noise and cluster sizes are temperature dependent and, if stable, noise can be easily subtracted from the data. Various types of cooling for the calorimeter were investigated by Ákos Sudár [18], and air cooling for the tracker was investigated as part of thesis on C-E sheets by Fredrik Mekki Widerøe [19]. In the final design, the cooling is two-fold: a closed-loop water cooling for all the layers, and an open-loop air cooling for the tracker layers and transition cards.

2.3.3 Challenges with Cooling

Cooling the DTC with water at the edge of the layers presents a problem with uneven heat distribution across the layers. While this is partly remedied in the tracker by forcing air movement across the layers, the same argument can't be made for the calorimeter. For this reason, investigating how temperatures are inside the calorimeter in the current mock-up are important.

2.3.4 Water Cooling

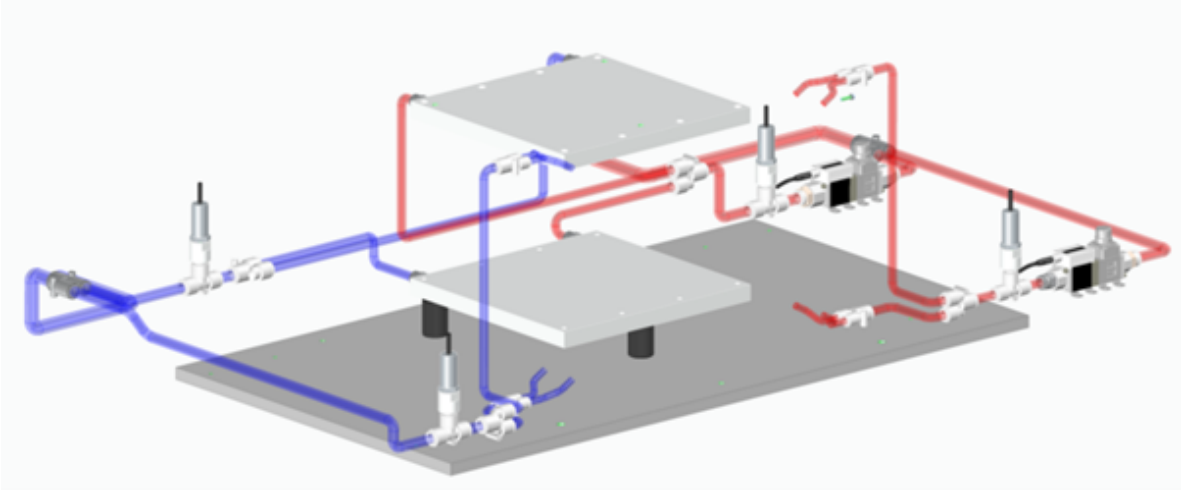

Figure 5: 3D Model of water cooling circuit through the tracker (front of image) and the calorimeter (two white plates in the middle). Blue represents the supply lines, Red represents the return line [3].

Water cooling is a system consisting of a chiller, a pump and plastic tubes. Water is chilled to a specified temperature in the chiller and is then pumped through the pipes to the DTC. On the way there is a splitter which lets roughly 20% of the flow through the tracker cooling pipes, and the other 80% through the two calorimeter cooling plates, found from the ratio of the calorimeter and tracker flow rate in table 3. At nominal values, discussed in chapter 4.2, the energy consumed in the calorimeter will be 20 times larger than in the tracker, thus requiring more water to cool it down. After flowing through both parts, the pipes merge and return into the tank to be chilled again. Water cooling is designated to cool ALPIDE sensors only, in both the tracker and the calorimeter.

2.3.5 Air Cooling

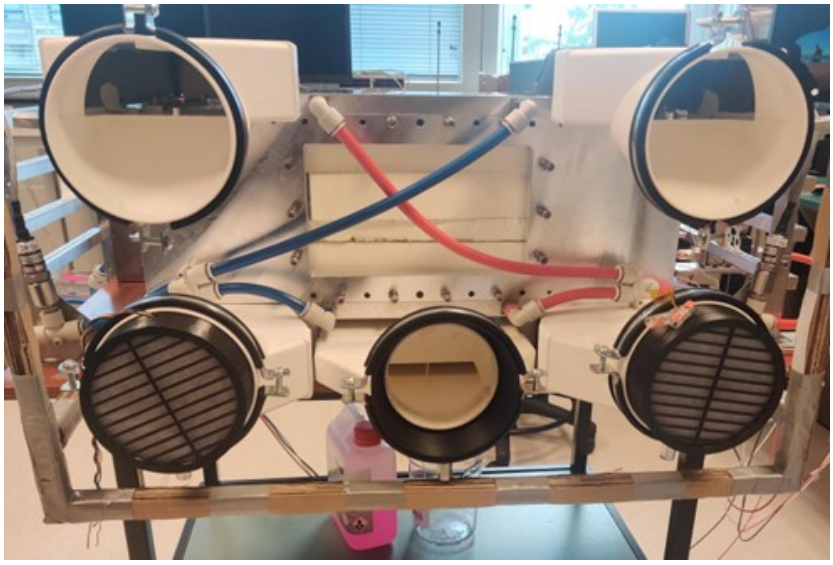

Figure 6: Early photo of DTC backside. The fan setup is visible, with intakes at the bottom and exhausts at the top. The 3rd fan goes in the middle and blows air through the tracker from below.

Air cooling is a simple system with three fans cooling transition cards and tracker layers hotspots using forced air. The fans are positioned at the back of the DTC. Two of these, both 125 mm in diameter, are configured for the calorimeter on the left and the right side. Air is pushed into the chassis from the bottom, and exhausted through the top cooling the transition cards. The third one, size 100 mm in diameter, is positioned in the middle pushing air towards the front in a tunnel below the calorimeter chassis, cooling the tracker ALPIDEs from below. While the water is expected to keep the tracker layers cool enough, the addition of air supplements it well by helping in avoidance of hotspots across the layer.

2.4 Briefly on the Cooling System Electronics

The cooling system electronics consists of following elements; power supplies, sensors, readout I/Os and an external storage device. These parts were part of this thesis, and are given a short breakdown here, else look to chapter 5 for a detailed breakdown. Naturally, power supplies supply every part of the cooling system with power. Flowmeters, pressure sensors and temperature sensors constantly gather data which are read by the readout I/Os, Moxa E1200 series I/O modules [20]. Then, everything is sent to a computer, running software which is constantly monitoring the system state, and

acting on any sudden changes in it.

2.5 List of Hardware Used for this Thesis with Specifications.

Table 1: List of hardware with part name, manufacturer name, their ranges and other important information.

Name	**Manufacturer**	**Range & Accuracy**	**Other Info**
LAUDA UC4	LAUDA	Out: 0 to 13.8 L/min	Circulation chiller with adjustable flow rate
Heating Strips	Custom Made	-	Tracker Heating Elements Equal to an ALPIDE *string*
M5131-70010X-4BC	MWS Sensorik	-1 to 3 bar ± 1%	Pressure Transducer, Out: 0.5 to 4.5 VDC - - Ratiometric
ioLogik E1212	MOXA	-	Universal I/O, Channels: 8 DIs and 8 DOs
ioLogik E1240	MOXA	-	Universal I/O, Channels: 8 AIs
ioLogik E1260	MOXA	Resolution: 0.1 °C	Universal I/O, Channels: 6 RTDs
PF3W504S	SMC	0.5 to 4 L/min ± 3%	Vortex flowmeter with inbuilt temperature sensor
PF3W520S	SMC -	2 to 14 L/min ± 3%	Vortex flowmeter with inbuilt temperature sensor
RS Pro Silicone Heater Mat 500W	RS Components A.S.		Calorimeter Heating-Elements Size: 10” x 10”, Input: 230VAC
RTS-M06-L050-K01 (1000).0668	EMKO Elektronik A.S.	-50 °C to 200 °C ± $(0.3 + 0.005\|T\|)$	PT-1000 RTD Sensor, Tolerance: Class B 3-wire

2.6 Status at the Start of 2022

Prototype status, per 2022, is that it is partly assembled. The calorimeter chassis and temporary tracker frames were in place, with parts of the cooling systems missing. The temporary heating solutions for both parts of DTC were already mounted. This was work that was mainly done by two members of the Bergen pCT Collaboration, Ton van den Brink and Shruti Vineet Mehendale. A lot of major hardware related to cooling was still missing. Including all the necessary readout hardware, some sensors and all the software. This laid the groundwork for most of this thesis, mainly assembly and testing of parts and the system they make together.

3 Thermodynamics and Fluid Dynamics

This chapter will briefly discuss the thermodynamics and fluid dynamics of the system. It will provide basic knowledge on some of these concepts and in what context they apply to the DTC. Herein, used formulas, basic material properties and assumptions made. The DTC itself is a complex system when it comes to those two concepts and theorizing on its exact properties would require time and resources that simply didn't belong in this work. For this reason, only simplified formulas are presented, which are used for calculating results throughout this thesis, especially chapter 8.

3.1 Simple Model for Thermal Stabilization Time of the Calorimeter

The final DTC prototype will be a lot more massive in both the tracker and the calorimeter. If we first consider the calorimeter is expected to be at 34.5 kg aluminium, while the current testing build is at 7.5 kg aluminium [3], there are other materials in the calorimeter, with comparetively small mass to aluminium, their masses are mostly unknown and are ignored simplicity.

In order to make a simple prediction of increase in thermal stabilization time, we only need to know the ratio of final mass with respect to current mass, as the power provided is controlled and can be expected to be equal in both cases. In short, to find how long the final mass of the DTC takes to stabilize, we only need to measure the time it takes in the current build and multiply it by the ratio of masses. Going by:

$$Q = m\Delta T C_p \tag{1}$$

Where Q = Heat/Energy, m = the mass, ΔT = change in temperature, C_p = specific heat

Taking the ration, we see that ΔT and C_p remain constant and cancel out, so the ratio is constant as long as masses do not change:

$$\frac{Q_2}{Q_1} = \frac{m_f}{m_c} => \frac{m_f}{m_c} \tag{2}$$

Q_1 and Q_2 are energies before and after change in mass respectively

m_c and m_f are masses in the current and the final prototype respectively

So now we only need to measure the current thermal stabilization time and multiply it by this ratio:

$$t_{final} = t_{current} * \frac{m_f}{m_c} = t_{current} \tag{3}$$

t_{final} and $t_{current}$ are final and current thermal stabilization time respectively. This ratio will be $\frac{m_f}{m_c} = 4.6$ for the calorimeter.

The tracker doesn't need to be considered in the same way. The only difference will be in what the layer will consist of. Currently, the layer mass is the aluminium frame and aluminium plates, which the heating elements are glued to, with a total mass of 314 g, emulating the C-E sheets. In the final prototype, this mock-up will be replaced by an aluminium frame with C-E layers, with ALPIDE sensors glued to them, giving a total mass of 332 g. This gives an 18 g difference, which isn't going to make a noticeable difference in thermal stabilization time.

3.2 Estimating Total Power Removed

There are two main ways heat is removed from both the tracker and the calorimeter. First is by thermal conduction to a liquid coolant and the second by convection to the air. At this point the heat distribution isn't important, we are rather interested in the total heat we are transferring through both liquid and air. For this, we can use two simple formulas. First is the heat transfer formula for the liquid cooling:

$$Q_L = \dot{\boldsymbol{m}} C_p \Delta T \tag{4}$$

Q_L is the heat transferred in the liquid (J/s)

$\dot{\boldsymbol{m}}$ is the mass per unit time (kg/s)

C_p is the specific heat of the liquid (J/kgK)

ΔT is the temperature change of the liquid (Kelvin)

Second, there are also some amounts of heat transferred by air convection, which is highly dependent on the surface temperature and air temperature. For this work, only

the free convection is considered. The formula for convective heat transfer (Newton's Law of Cooling) is:

$$Q_A = hA\Delta T \tag{5}$$

Q_A is the heat transferred in the liquid (J/s)

h is the convective heat coefficient (W/m^2K)

A is the are of convective surface (m^2)

ΔT is the temperature change of the liquid (Kelvin)

In the tracker the heat transfer is more evenly split between conduction and convection, in comparison to the calorimeter where conduction is dominating. This is caused by the ratio of energy to surface area and will be discussed later.

Radiative heat transfer is ignored in the tracker and calorimeter, as it is negligible in both cases at the temperatures of interest.

3.3 Estimating Total Supplied Power

Estimating the total power in the DTC is just as important as estimating how much heat is removed. Knowing this value approximately gives insight into how well the cooling system performs. The heat generated comes mainly from the heating elements, pads in the calorimeter and strips in the tracker, as well as by mechanical power of the coolant itself. Also, although rather small, the system will gain energy whenever the surface temperatures are lower than environmental air temperatures and will also be considered in these cases using the aforementioned Newton's Law of Cooling.
Estimating mechanical power of the flow can be approximated from pressure and volumetric flow rate:

$$P_M = PV \tag{6}$$

P_M is the mechanical power (W)

P is the supply pressure (N/m^2)

V is the volumetric flow rate (m^3/s)

3.4 Power from Heating Elements

The heating pads resistance was measured to be 107.7 Ω for the top heating pad, and 105.4 Ω for the bottom one. The heating pads, which are parallell to each other, are routed through a multimeter, so the total current through the pads is measured in real time, and the power is regulated using that current readout. In the lab, the voltage is varied using an AC voltage regulator and the resistances are constant, we need to calculate power off of change in current. Power delivered to each pad is given:

$$P_N = R_N I_N^2 = R_N (I_M \frac{R_{eq}}{R_N})^2 \tag{7}$$

R_N, I_N, P_N are circuit resistance (Ω), current (A) and power (W) respectively

I_M is the current at the multimeter

The equivalent resistance R_{eq} in this simple parallel circuit is given by:

$$R_{eq} = R_N (I_M \frac{R_T R_B}{R_T + R_B})^2 \tag{8}$$

R_T, R_B are the resistances through top pad, bottom pad respectively

I_M is the current at the multimeter

The total power P_E to the heating pads is then given by using the equivalent resistance, or by addition of power for each heating pad with power loss in the multimeter subtracted:

$$P_E = P_T + P_B - P_{MM} = R_{EQ} I_M^2 - R_{MM} I_M^2 \tag{9}$$

P_E is the electrical power to both heating pads

P_T, P_B, P_{MM} are the power through top pad, bottom pad and power loss in the multimeter respectively

Calculating the power to the heating strips on the other is not necessary, due to use of a precise power supply. So P_E in that case is the power read from the power supply.

3.5 Heat Removed by the Coolant

Now that we can estimate both the supplied and removed power in the system, we can put them together to check how much heat the liquid coolant is removing.

$$Q_{supplied} = Q_{removed} => Q_L = P_E + P_M + Q_A \tag{10}$$

What this equation tells, is that at the temperature equilibrium point, the energy removed by water equals the total energy supplied by the heating + total mechanical energy of the flow + the energy, either supplied or removed depending on direction of convection, by air, per unit time.

When considering the uncertainty equation 10 using measurements considered in chapter 6.4 and 7.6, the uncertainty of $Q_L >> P_E$ *or* P_M *or* Q_A, in the order of 100 to 1. For simplicity, uncertainty of Q_L is the only one considered.

First, in order to eliminate the systematic error of temperature measurement, as the PT-1000 sensors are tolerance class B, we change ΔT in equation 5:

$$\Delta T_{real} = \Delta T_1 - \Delta T_0 \tag{11}$$

ΔT_0 is the temperature difference between water inlet and outlet shown with no flow, which after calibration is the same value. ΔT_1 is the actual temperature measurement when water is flowing with a certain flow rate. This way the systematic error cancels out, and we remain only with the error caused by resolution of MOXA E1260, at 0.1 °C.

In an ideal scenario, both sides of the equation would be equal. However, it is fully expected that there will be some deviation from this equality in equation 10, which can then assist in finding where eventual, theoretical shortcomings came from.

3.6 Estimating Temperature Drop Across an Absorber Plate

Estimating temperature drop across an absorber plate is done by using Fourier's Law of Heat Conduction to calculate resistance of the plate, then multiplying it with nominal power of each ALPIDE sensor on it. This shows the upper limit of this value, as it assumes all sensor on one side. First:

$$R_\theta = \frac{t}{Ak} = \frac{0.1m}{0.0029m^2 * 220\frac{W}{Km}} = 0.157\frac{K}{W} \tag{12}$$

R_θ is the thermal resistance (K/W)

t is the height of the absorber plate (m)

A is the area of connection between absorber plate and cooling plate (m^2)

k is the thermal conductivity of absorber plate material (W/(mK))

Given $A = 0.0029\ m^2, t = 0.1\ m, k = 220\ W/(Km)$ for $> 99\%$ pure aluminium.

Each half-layer will contain 54 ALPIDEs, each with a nominal power of 0.202 W, this give a temperature change across the plate to be:

$$dT = R_\theta * P_{ALPIDE} * 54 = 0.157\frac{K}{W} * 0.202W * 54 = 1.71K \tag{13}$$

dT is the expected temperature change (K)

R_θ is the thermal resistance (K/W)

P_{ALPIDE} is the nominal power of an ALPIDE chip (W)

3.7 Fluid Dynamics

The fluid dynamics of the DTC are quite complicated and would be better reserved for another thesis with proper simulations. However, basics of how the type of flow affects the heat coefficient of the coolant is necessary to properly evaluate the results of various heat measurements. The most important factor at play is the Reynold's Number Re, indicating the type of flow present, which can be evaluated from flow and liquid properties:

$$Re = \frac{uL}{\upsilon} = \frac{\rho u L}{\mu} \tag{14}$$

u is the flow speed (m/s)

L is the linear dimension of in this case, the tube (m)

υ is the kinematic viscosity of the liquid (m^2/s)

μ is the dynamic viscosity of the liquid (kg/ms)

ρ is the fluid density (kg/m^3)

Water is assumed to have $\rho = 1000\ kg/m^3$ and $\mu = 1 * 10^{-3}\ kg/ms$. Here, the considered diameter of tube is the one at the cooling segment itself, so the one in transferring heat to the liquid. For the calorimeter, the tube diameter is 12 mm at the cooling plate is and for the tracker, the tube diameter is 9 mm.

3.8 Importance of High Reynold's Number

The type of flow greatly affects how well heat is transferred from the tube walls to the water coolant. The type of flow is found by calculating Reynold's Number, using equation (14) above. Generally, in pipe systems, $Re < 2300$ means the flow is laminar, transient or critical for $2300 < Re < 4000$, and turbulent for $Re > 4000$. Laminar flow causes the fluid to move smoothly, in an orderly fashion. This means little to no mixing between layers, as the heat transferred into the outer layers of water stays there causing in turn less absorption by those layers, resulting in an overall lower heat transfer coefficient. Turbulent flow on the other hand is disorderly and chaotic, layers mix, meaning heat transferred is spread out into the whole liquid stream leading to a comparatively higher heat transfer coefficient. Therefore, in general we want the flow to be turbulent to raise the efficiency of the cooling system.

3.9 Important Assumptions

There are a few important assumptions made in this work that need to be mentioned. These will later be discussed together with results, presenting a couple obvious problems which might be responsible for uncertainties in results.

- The tracker and the calorimeter are always assumed to be completely independent of each other, meaning no heat and cooling contributions are made from one to the other.
- The heat is assumed evenly spread out throughout the whole mass/surface area when calculating convective heat, unless specified.
- The Reynold's number, and mechanical power are calculated from return pressure and volumetric flow rate.
- The flow is assumed to evenly split between parallel pipes. This means that the 80% of the water that goes through the calorimeter, splits evenly between both cooling plates, and the 20% of the water that goes through the tracker splits evenly between all four tubes.

4 Requirements of Hardware and Software

When building any machine, one usually must adhere to certain criteria, restricting aspects of it. This is especially true in the medical field, where standards for any device are extremely high in order to ensure safety of both the personnel and the patients, as well as robustness during long working hours. This chapter will give context as to why certain design decisions were made for the Bergen pCT Project. This includes the safety settings for the ALPIDE chips, requirements of the water- and air-cooling systems, hardware limitations and software requirements. Some expected, simulated system parameters will also be presented. All of the above outline the baseline problems this thesis attempts to resolve.

4.1 Safety Settings

Bergen pCT Digital Tracking Calorimeter will consist of 4428 ALPIDE sensors. Even though most of them won't be running at full power simultaneously at any given time, they are all idling waiting for particle hits. ALPIDE sensors get noisier the higher the temperatures are, therefore the temperatures should be kept as low as possible for optimal particle detection and for the noise to remain at roughly constant values. Transition cards, on the other hand, are allowed to reach higher temperatures, and will therefore be only cooled using the air cooling.

4.1.1 Temperature Safety

Temperature safety, as a concept, describes temperature limits of various parts of the DTC and the automatic systems response to them. These limits are presented in table 2 for ALPIDEs, transition cards and air surrounding transition cards, called "Transition Card: Air". There are two temperature thresholds at which the system acts. First is the lower temperature limit, called ***HIGH***, at which a temperature warning is generated in the distributed control system (DCS) for the user giving possibility of manual intervention. Then a higher temperature limit, called ***HIGH HIGH***, at which the decision support system (DSS) automatically shuts off power to the DTC chips.

Table 2: Temperature limits for ALPIDEs, Transition Cards and air surrounding the transition cards

	ALPIDE	**Transition Card**	**Transition Card: Air**
HIGH	35 °C	45 °C	40 °C
HIGH HIGH	40 °C	50 °C	50 °C

4.1.2 Fan Vibration

When air cooling is running, the fans will produce some amounts of vibrations at various frequencies. These vibrations, specifically in 75-150 Hz range, present a direct danger to the tracker layers. In order to prevent damage to them, fans will therefore receive an additional support frame, mounted to the calorimeter chassis. This will help reduce vibrations, and thus prevent damage to the tracker, by giving the fans a stiff support.

4.2 Maximum ALPIDE Energy Consumption

ALPIDE sensors each have a nominal power consumption of 0.202 W. In the calorimeter there are a total of 41 layers, each layer with 12 *strings*, and each *string* with nine ALPIDE sensors on it. This gives a nominal power in the calorimeter:

$$41 * 12 * 9 * 0.202\ W = 894.456\ W \approx 895\ W$$

In the tracker there are two layers, each with 12 *strings*, and each *string* with nine ALPIDE sensors on it. This gives a nominal power in the tracker:

$$2 * 12 * 9 * 0.202\ W = 43.632\ W \approx 44\ W$$

4.3 Water Loop Limitations

Certain parts of the water-cooling loop have limits which will inhibit the number of adjustments to flow through the machine that could be made. First off, the pressure sensors have a P_{max} of 3.5 bar. Now, there isn't any immediate damage done to them if the pressure is momentarily above that value, but if sustained, there are risks of that. Therefore, the system must be adjusted to always keep below this value. Similarly, the polyuretane tubes and connectors have a P_{max} of 6 bar, at which point some leaking and possible cooling loop damage is expected.

4.4 Simulated Cooling System Parameters

Both of the cooling solutions are expected to meet certain theoretical parameters. These parameters are supposed to meet a specific change in temperature per unit time, which in the calorimeter is 2 °C per cooling plate and in the tracker is 0.2 °C per cooling tube. They can be found in the table below. The values might be slightly misleading, as they serve only as suggestions, pointing to somewhat expected values in the actual cooling system. So, they were used as a soft guideline in tweaking of parameters found in table 4.

Table 3: Table of simulated water and air cooling parameters, provided by [3].

Part	**Setting**
Tracker Flow Rate	3.2 L/min
Calorimeter Flow Rate	13.6L/min
Lauda Temperature	18 °C
Expected Tracker Air Flow Velocity	4.8 m/s
Expected Transition Card Air Flow	120 m^3/h

4.5 Achieved Water Cooling Parameters

Keeping in mind the pressure sensor pressure limit of 3.5 bar, the parameters found in table 4 were achieved at the current setup at maximum flow output of the chiller pump, this was achieved by regulating flow meters valves, described in 5.4. Currently the flow through the tracker is larger than expected and the flow through the calorimeter is lower than expected, discussed further in chapter 8.5. The total flow in the system is more than the chiller technical specification specifies. This is explained further in chapter 6.2.3.

It is important to know that the system is not recommended to run this close to the pressure limit, so at maximum chiller flow output. This is because the pressure transducers are above their range and their output might not be as accurate, meaning it is possible the pressure is above 3.5 bar.

Table 4: Table of achieved water cooling parameters.

Part	**Setting**
Tracker Flow Rate	3.36 L/min
Calorimeter Flow Rate	12.05 L/min
Calorimeter Supply Pressure	3.18 bar
Calorimeter Return Pressure	2.65 bar
Tracker Supply Pressure	3.41 bar
Tracker Return Pressure	3.32 bar

4.6 Sensor Requirements

The precision and accuracy required of the DCS sensors can be split into two parts, the live monitoring and system characterization. The monitoring itself has lax requirements dependant on the sensor. Within a one-tenth for the flowmeters with inbuilt temperature sensors, as these will have values in tens and ones, for example 10 L/min and 20 °C. For the pressure sensors accuracy within one-tens would more than suffice, as the values are usually in thousands, for example 2500 milibar. Measurements for the characterization of the mock-up would require more precision to reduce error as much as possible. Generally one order less, so one-hundredths for the flowmeters and one-ones for the pressure sensors, would be good enough. For every permanent sensor, both requirements were fulfilled. The temporary PT-1000 sensors were of tolerance class B, which is good enough for most measurements in chapter 7. However, for the measurement of the change in coolant temperature in chapter 7.6, 8.1.1 and 8.2.1, this systematic error cancels out and only the resolution of MOXA E1260, at 0.1 °C remains as a limiting factor, causing a large error in calculation of energy absorbed by coolant.

4.7 Software Requirements

Monitoring any given cooling system for any type of machine is as important as the machine itself. Given how fragile ALPIDE sensors are, tracking any sudden changes and acting upon them quickly is crucial. For this project it was concluded that both a live data display to the user and an autonomous shut-off procedure will be employed,

the former being a part of the DCS and the latter the DSS. The DCS can only display warnings the user, upon which manual action must be taken. On the other hand, the DSS is independent of that, serving as an autonomous protection of ALPIDEs, in case of extreme changes in the system, like sharp temperature rises or loss of coolant flow.

The requirements for the software were not that uncompromising. As long as it could readily control the cooling system, by sending and receiving data through MODBUS, it was good enough. The considered programming languages, in which the DCS and DSS could be written, were C++ and Python. Due to the use of Python in database implementation by Håvard Birkenes [21] which this project will take advantage of, the ease of working with python and the small amounts of data transmitted, it was concluded that Python is the best choice as programming language between it and C++.

5 Electronics, Readout and Operation

Naturally, there will be some deviation from simulated system parameters. For this reason, some practical work must be done on the system, testing it to find out how it behaves. Most work of this thesis focused exactly on how the cooling system is performing in practical scenarios. This chapter will focus on how the system was expanded with various sensors and readout units, and then explain how they are operated and regulated. Readout from the DCS will be discussed.

5.1 Detector Cooling System Electronics

This section will briefly describe how the DCS system was expanded with power supplies, various sensors and readout I/Os. Preparing and mounting the hardware was done jointly with Tea Bodova, a current PhD candidate.

5.1.1 The Power Supplies

Power supplies provide necessary power for all the DCS electronics and are visible in figure 7. There are three in total: one 24 V, one 12 V and one 5 V, supplying different parts with power. The 24 V power supply supplies electricity to the Moxa I/O modules. The 12 V power supply provides electricity to the fans in the air cooling. The 5 V power supply provides electricity to all the sensors. All of them are connected to one power outlet, as the power draw of all the components together is rather small even at peak usage.

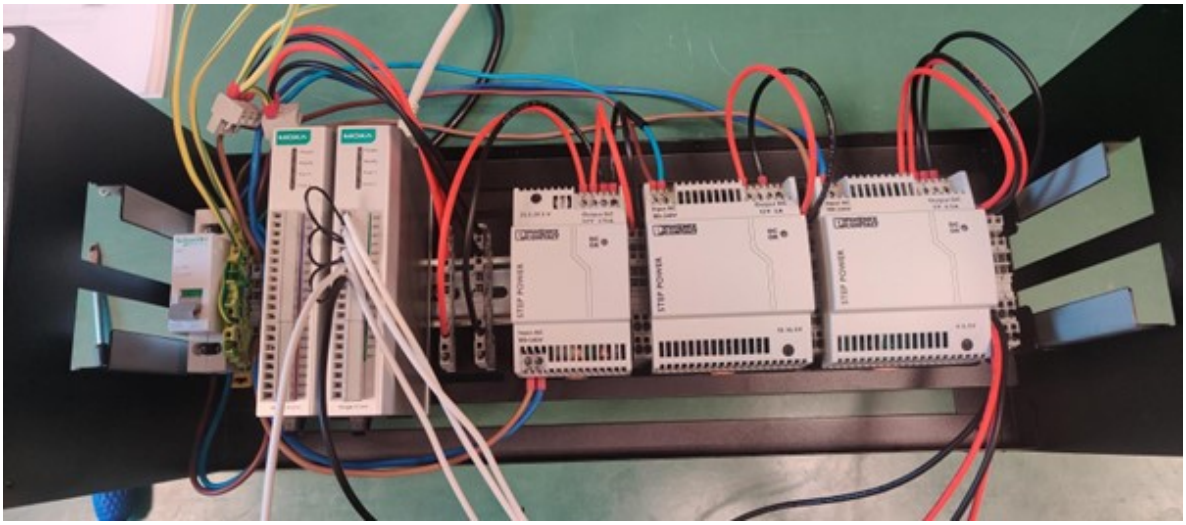

Figure 7: Photo of Moxa I/O modules (from left to right; E1212 - E1240) and power supplies (from left to right; 5V - 12V - 24V). The temporary MOXA E1260 not included.

5.1.2 The Cooling System Sensors

There are a total of eight sensors in the DCS, constantly collecting system parameters. There are four pressure sensors, outputting an analog voltage signal. These are pairwise positioned at water supply lines and water return lines, for tracker and calorimeter water cooling. They measure pressure when the water enters each DTC part, and when it exits.

Positioned right after the water-return pressure sensors are the flowmeters. Flowmeters constantly measure the amount of liquid flowing through them, collectively giving the amount of water flowing through the system at any point in time. These are of the vortex meter design, giving fast and quite precise measurements. Included are regulators valves, allowing regulation of flow through each flowmeter. Both flowmeters also come with an inbuilt temperature sensor, allowing the monitoring of water temperature in the system. Flow and temperature sensors both output an analog current signal.

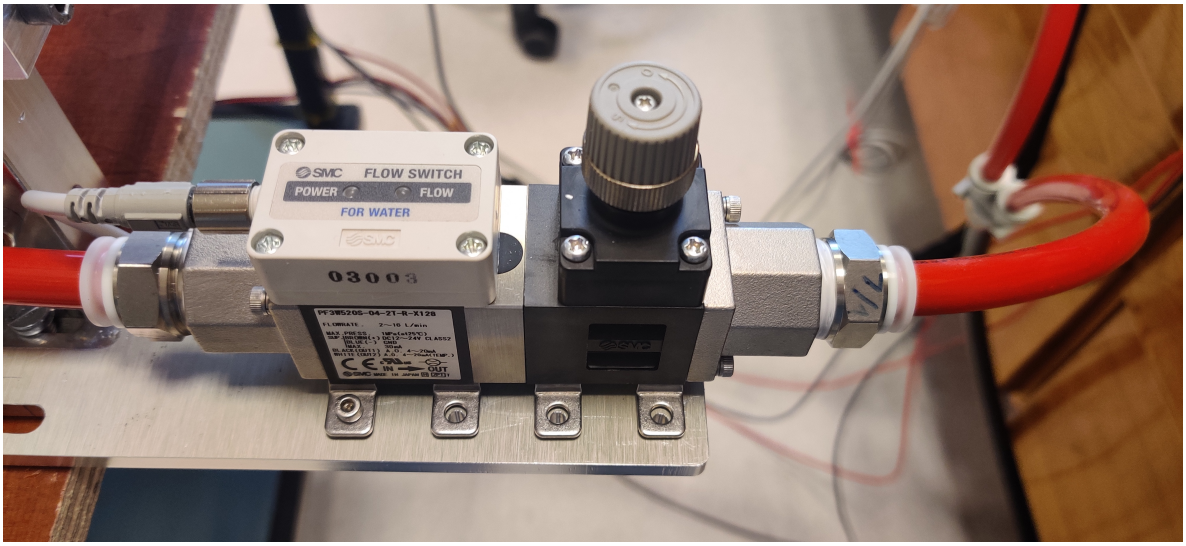

Figure 8: Image of flowmeter, left side (metallic) is the meter itself with the temperature sensor, right side (black) is the regulator valve.

5.1.3 PT-1000 Sensors

To measure temperatures at different points in the machine, six PT-1000 sensors were used. These were used only for the purpose of this thesis and are not part of the final DTC design. In order to check the performance of the cooling systems the temperature was measured at different points, using these sensors.

5.1.4 The Readout I/O Modules

The readout from the sensors happens by utilizing three MOXA universal I/Os, partly visible in 7.

First module, the E1240, is responsible for collecting analog signals from the pressure sensors and the flowmeters. This module has eight channels, with each being able to either read voltage or current analog signals. By default only voltage signals are read and must be switched to current mode if the signal is a current. The switch is manual and the module must be opened in order to switch it. This is required for signals from the flowmeters.

The second module, the E1212, is digital with eight digital input and eight digital output channels and is only used for fan speed control. Fan control is done using pulse width modulation.

The third module, the E1260, is responsible for measuring temperatures in points of interest. It has six Resistance Temperature Detector (RTD) channels and to each channel a PT-1000 sensor is connected.

5.2 Further Data Processing

Data from Moxa I/O modules is digitized and needs to be further processed into easy-to-read physical parameters. Current requirement for data conversion is any computer capable of running Python scripts. Data is first converted using calibration formulas obtained from calibration procedures, explained in chapter 6. Data is then sent into a database and displayed for the end user, requiring additional software. This is explained further in chapter 5.

5.3 System Operation

System operation is quite straightforward and can be condensed to powering up the system and starting the readout software. However, a more in-depth description of operating each part of the system and each step before measuring is quite important to understand, as at this stage in the building of the DTC, the setup isn't very user friendly for uninformed users.

5.4 Valve Regulation

Valves are essentially the only way to physically control the DCS. There are a total of three regulation valves in the water loop, each is adjustable from fully open to fully closed and determines how much water will flow through each part of the system.

5.4.1 Chiller Pump Regulation Valve

First is the chiller pump regulation valve, found by removing the chiller top cover, positioned under the electronics housing. How open it is determines how much water enters the whole loop. The valve is of the ball-valve type, and valve opening versus fraction of full flow isn't linear. There is no good indicator showing how open it is, and one can only eyeball it. This means that any tests where the chiller pump valve is

adjusted to a position between fully opened and fully closed, can't be reliably replicated. Preferably, because of this property, it would be fully opened at all times. This is however the only valve which allows reduction of flow without increasing the pressure, important when looking at how water removes heat with various flow rates.

5.4.2 Flowmeter Regulation Valves

The other two regulation valves are positioned at the flowmeters. One for the tracker, and one for the calorimeter, both after the meter itself, see 8. Both valves are of the needle valve type [22], meaning valve opening versus fraction of full flow is assumed linear. Regulating these valves is reliable and can be done with a high degree of precision by looking at how the flow rate changes. One can also count the turns or note how high the knob itself is, but these methods are auxiliary and not practical when flow rate readout is available.

These valves are implicitly linked to one another as playing with one of them will influence the flow through the other. The cause and effect are quite straightforward. Restricting a path causes less fluid flow through it. This in turn will cause more fluid flow through the other path. Additionally, a change in pressure is expected while restricting the flow, which is the most important, limiting factor of the system.

5.5 PT-1000 Sensor Placement

Measuring temperature at specific points allows for gathering data needed to characterize the performance of the cooling system. Pt-1000 elements are very sensitive and should be all means be isolated from the environment. Encasing the sensors in isolation shields them from air movement, which would cool them through convection.

Generally, the measurement spots should to some degree align with position of elements in the finished DTC. This would allow to compare the temperatures to the ones obtained from simulations. While this is easily done for the tracker, as the heating strips distribute the heat throughout the whole layer very comparably to ALPIDE sensors, same can't be said for the calorimeter. In the calorimeter, the pads can provide more than enough heating power to emulate all the ALPIDEs running at nominal power, but their placement at the top and bottom cooling plate makes the heat distribution

different than in the final design. While this in itself isn't a very large issue, as the total power inside the calorimeter chamber is the same in both cases, the heating pads make it difficult to measure temperatures inside the calorimeter chamber at spots which are comparable to the final design. As an example, even though the aluminium absorber layers were available at time of testing, there were no good ways to place them such that they were both heated well and in similar amount of contact with the cooling plate as in the final design.

5.5.1 Tracker Spots

The spots chosen for the tracker are presented in figure 9. First, 9a) shows where the temperature of the water inlet and outlet was measured. Then, in 9b), one sensor was taped to the layer center, measuring what essentially is the hottest spot and one to the frame on the right just measuring frame temperature.

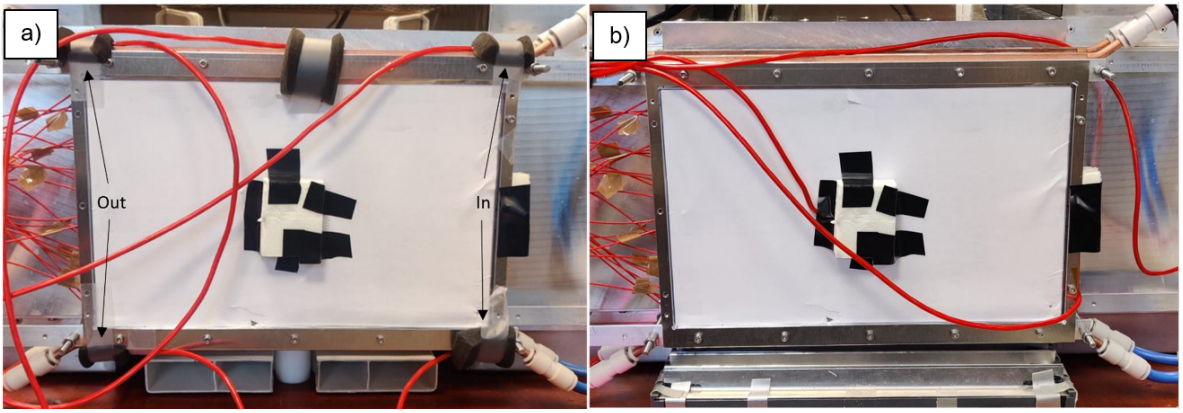

Figure 9: a) Positions of RTD sensors for measuring water temperature in the Tracker. «In» and «Out» show position of sensors at water inlet and outlet respectively. b) Positions of RTD sensors measuring tracker tempeartures, one at far right, the other in the center covered by polystyrene and black tape.

5.5.2 Calorimeter Spots

As mentioned earlier, choosing the spots in the calorimeter was more complicated. Therefore a decision was made to go for a slightly different approach than looking for spots that could be compared to simulations. The methodology revolved mostly on the

ALPIDE temperature limit. Given this limit, the spots where positioned and configured such that they reached as high of a temperature as possible whenever they were. This usually meant isolating them to prevent air exchange with the environment.
First, the temperature of the water inlet and outlet was measured for both cooling plates, see figure 10.

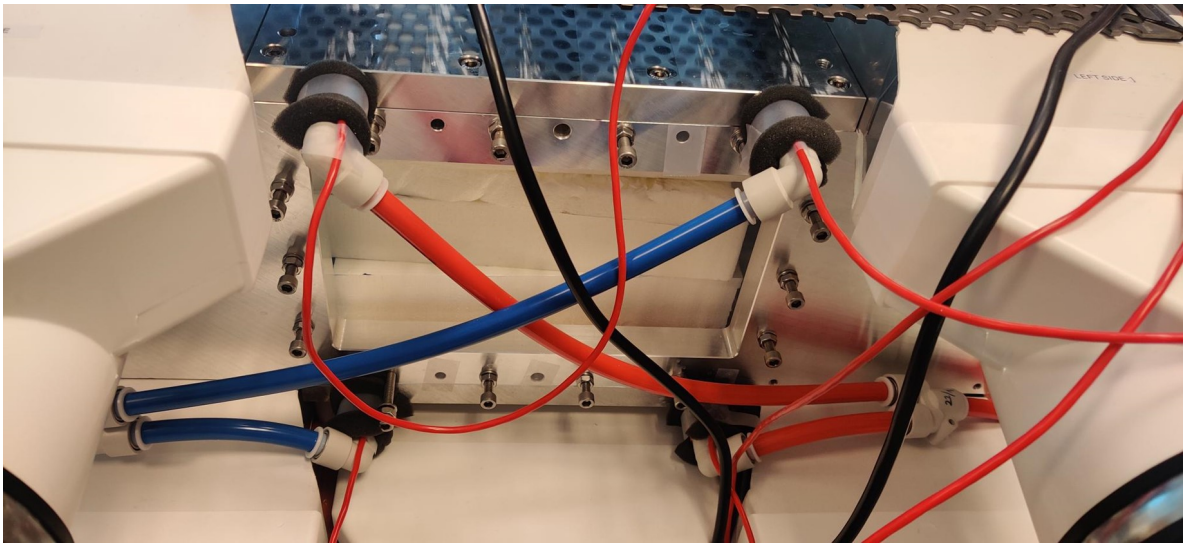

Figure 10: Back of the DTC, where water temperature at inlet and outlet was measured. Red cables lead to PT-1000 sensors, blue tubes represent inlets and red tubes represent outlets.

Then the air temperature at various spots was measured. First inside, along the center of the heating pad, as visible in figure 11 below. The block in figure 11B was individually made for top and bottom tunnel so that it fit tightly and could be moved along the cut-out tunnel. This allows for measuring of temperatures at various depths. The other end is plugged so that it doesn't leak air, however, it was not air-tight. The sensors were positioned such that they weren't directly above a coil on the heating pads. In this setup, two spots were chosen for both top and bottom. First is the center, the assumed hottest part, and the second is on the center side. The idea was simply to see what sorts of temperatures we can expect given little to none heat removal through air exchange.

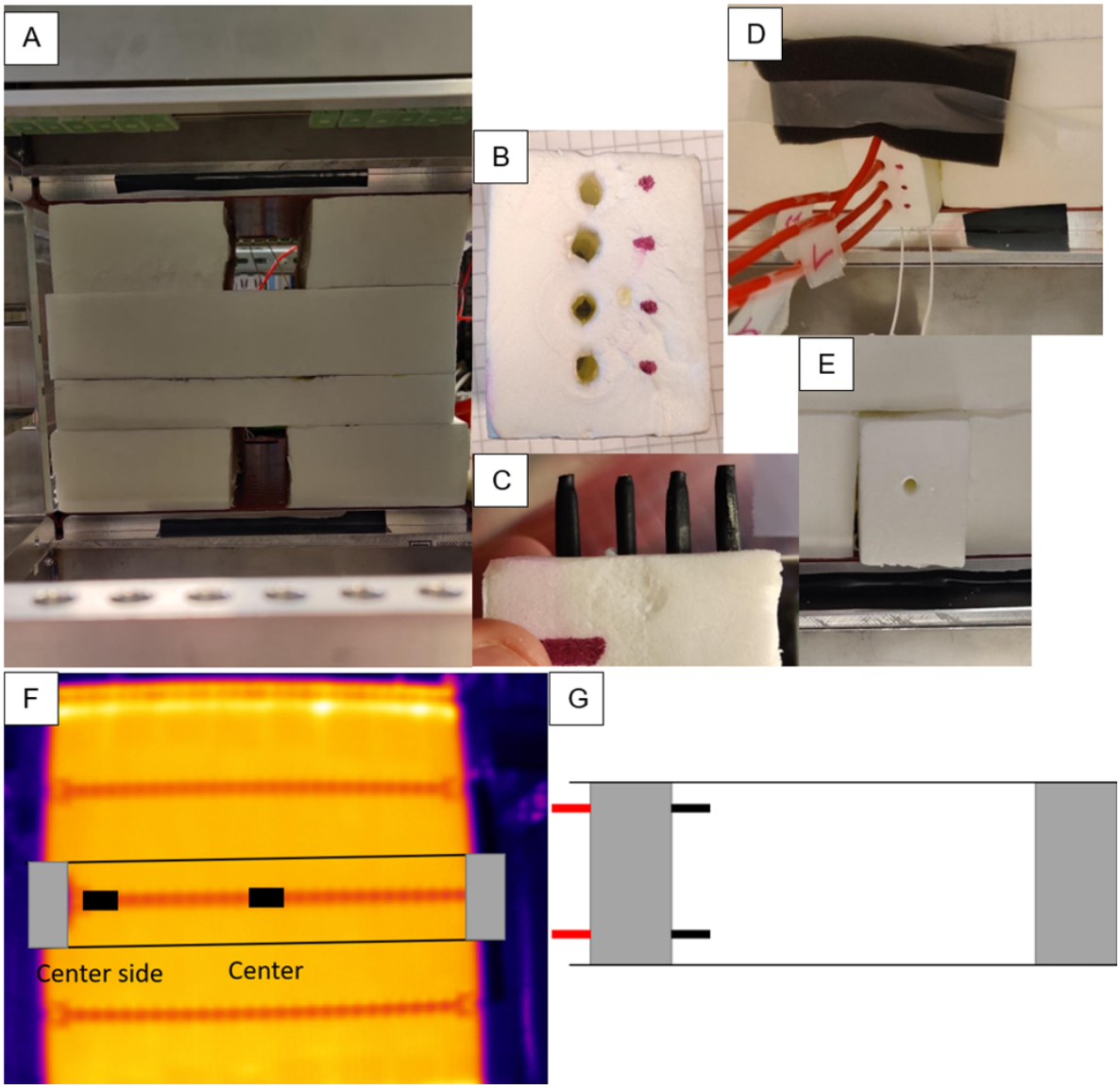

Figure 11: A: Polystyrene cut-out, can be adjusted, B: Polystyrene block housing the PT-1000 sensors, C: How the sensor look like in the block, D: Sensors inserted into the cut-out chamber, E: Polystyrene blocking the other side, gaps were later filled with black sponge material visible in D, F: Thermal image of the heating pad, shows where the sensors were positioned on the pad, G: Side view of the cut-out chamber with the sensors.

There is also two spots referred to as "hotspot" and "coldspot" in figure 30 and 31. Hotspot represents the center of the heating element, see figure 11F, with the PT-1000 sensor directly in contact with it. Coldspot represents the corner of the heating element, with the PT-1000 sensor 1 cm away from it, see 12.

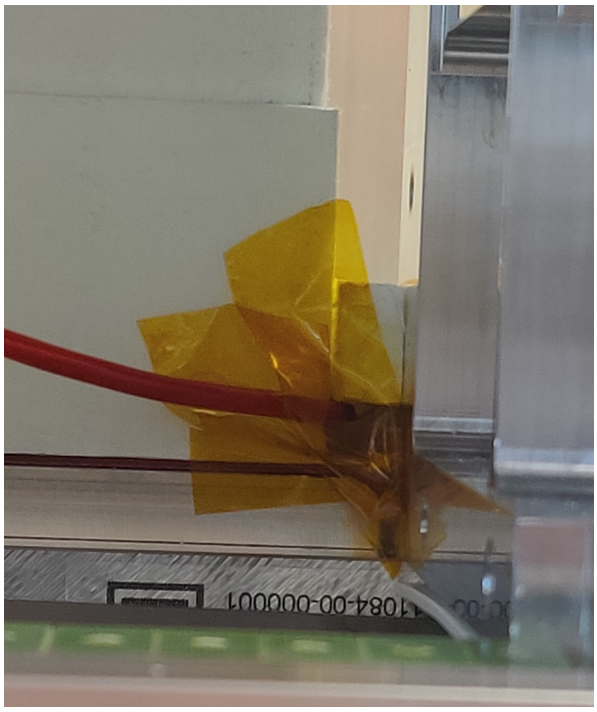

Figure 12: Image showing where "coldspot" PT-1000 was positioned, measuring air temperature inside a tape encasing preventing the sensor from being affected by air movements in the lab.

The last set of spots were positioned on an aluminium plate absorber. One plate was positioned at the back of the calorimeter chamber, with small area in contact with the heating pads and large area in contact with the aluminium chassis. The other was squeezed between the heating pads having small area contact with them and no contact with the chassis or the cooling plates.

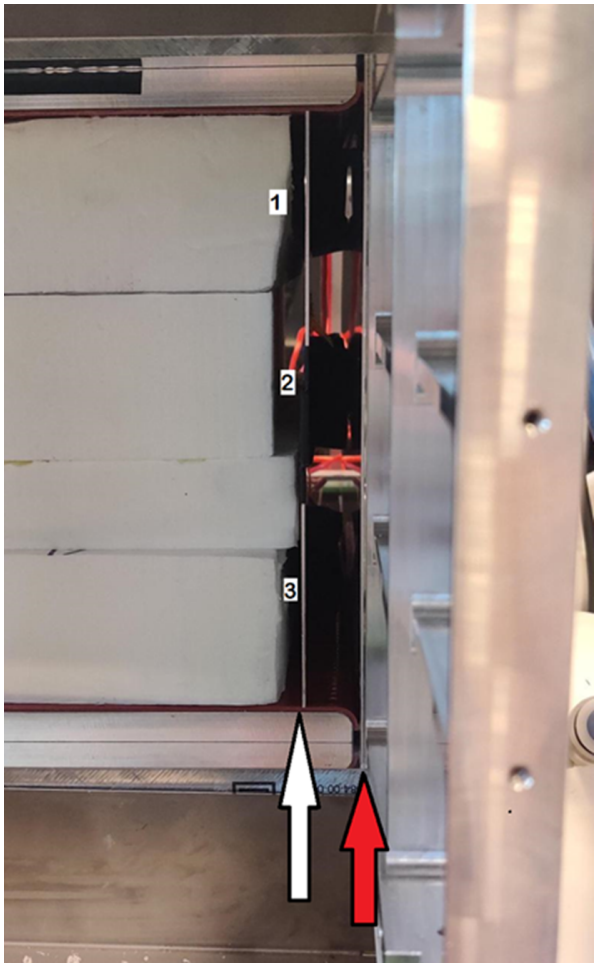

Figure 13: Position of absorber layers inside the calorimeter chamber. White arrow shows the absorber plate that didn't have any contact with the cooling plate. Red arrow shows the absorber plate which was in contact with chassis over larger area than the final design.

5.6 Data Collection and Readout

All the data collection happens automatically after powering up the system, only the readout software needs to be manually started. Readout software is a basic python script, at this point in time run through the terminal. All the data received from the Moxa I/O modules is first converted using formulas obtained from sensor calibration. An exception is the E1260 RTD Moxa I/O, which gives a direct temperature data that doesn't require conversion. Data can then be written to the database or to a text file. The database needs to be started, either manually through the terminal, or by using a script. Data can then be viewed, stamped with date and time, in either InfluxDB or

Grafana. It is formatted into cells, so importing it into programs like Excel is quick and easy.

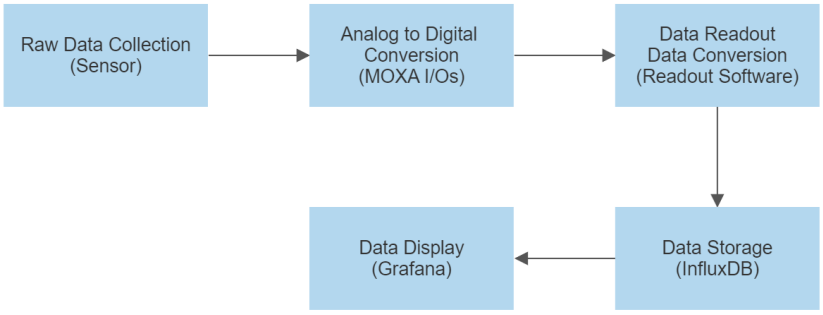

Figure 14: Software flowchart for Moxa E1240 and E1260, from sensors to display.

5.7 Using the Configuration File

The configuration file allows for changing of certain parameters for the readout script. First off, the ip of the MOXA units need to be specified. Then conversion formulas need to be specified, as data from Moxa I/Os is in a raw format, explained further in chapter 6. Lastly, there is an option for activating certain debug features, like outputting data to terminal or to a text file for further analysis.

5.8 Data Readout Results

In total, there are four different different methods of showing data collected by the MOXA I/Os. First, we have the optional display in a terminal or optional write to a text file, which can then be viewed or analyzed. Then, by default, a storage and display in InfluxDB and further a display in Grafana.

5.8.1 Terminal Output

The terminal output is very simple. As data is read its raw value and its converted value are both written to the terminal. This isn't particularly useful in analysis, and mostly used to check if everything is outputted correctly.

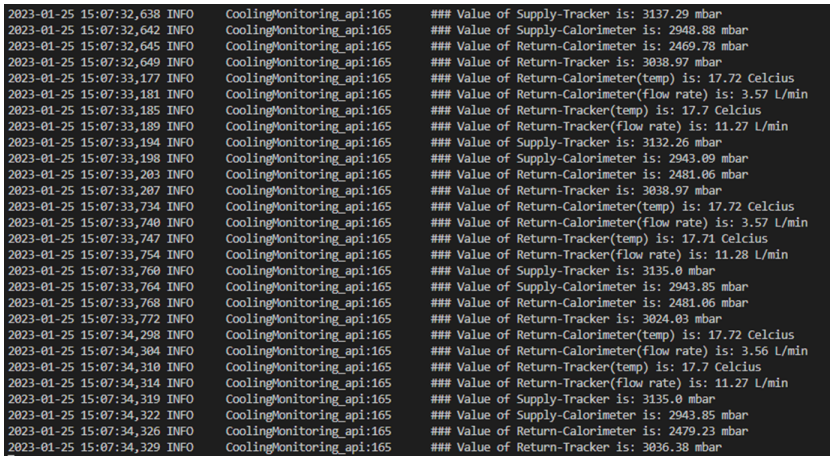

Figure 15: Terminal output for readout software.

If tagged in configuration file, it is also possible to write data into a text file. Same as before, both the raw value, and the converted values are included. Data is timestamped to make it easier to browse. Main reason for this option is for raw data analysis. Unlike parameters available from the database, the presence of raw data makes it ideal for tests requiring it, mainly used in calibration of flow rate, of the flowmeters.

5.8.2 InfluxDB Interface

Data in converted format is sent directly to InfluxDB. It is saved in the database and can be viewed any time the database is running. An advantage of InfluxDB is automatic data stamping, meaning less data needs to be uploaded from the readout script. Sensor data is saved in "layers", each layer represents data from a single sensor. As well as that data can be easily worked with using queries and scripts. Queries allow, for example, to take the mean during a period of time.

Figure 16: InfluxDB example of a single layer graph display in visual query mode. Graph display water temperature in Tracker flowmeter.

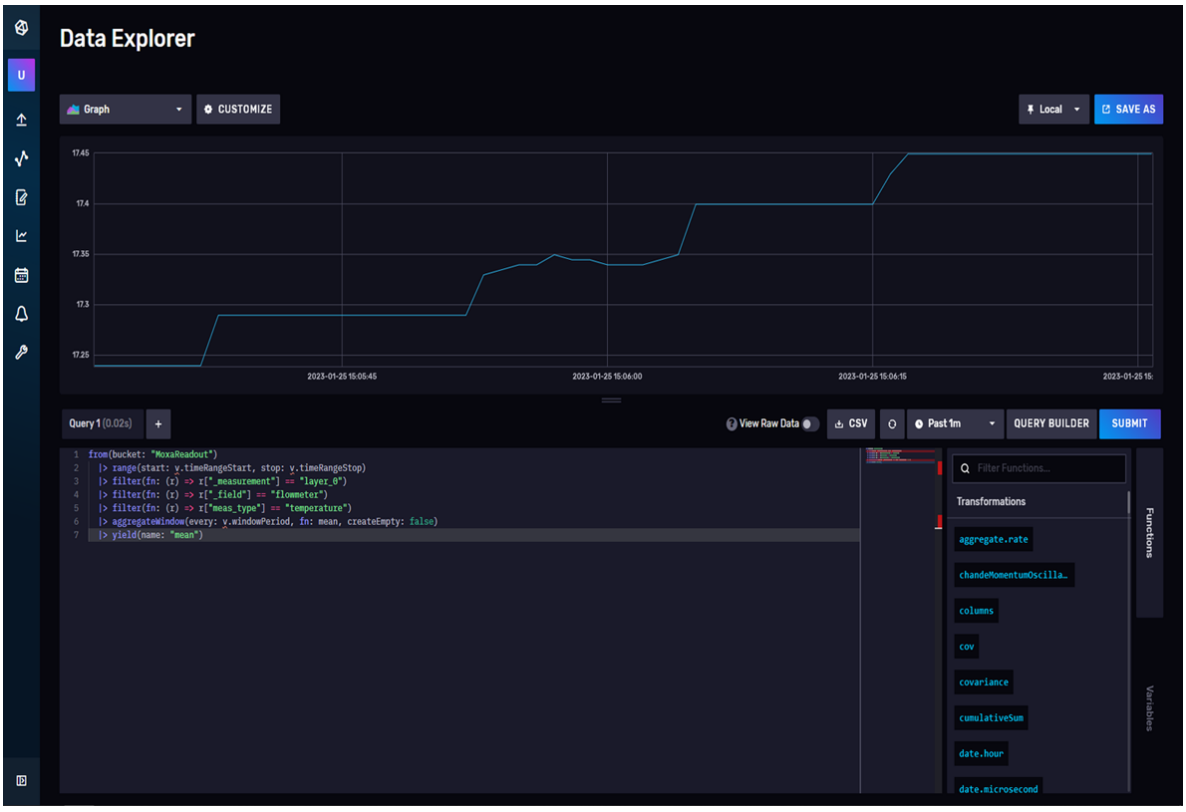

Figure 17: InfluxDB example of a single layer graph display in script mode. Graph display water temperature in Tracker flowmeter.

The interface of InfluxDB isn't very useful for displaying more than one type of sensor data. Specifically, only one graph window is available at a time, and all the chosen sensors will be plotted on it. Therefore, having two graphs showing different types of data makes them hard to read, and makes the y-axis make no real sense. Further, showing all eight DCS sensors at the same time is extremely impractical.

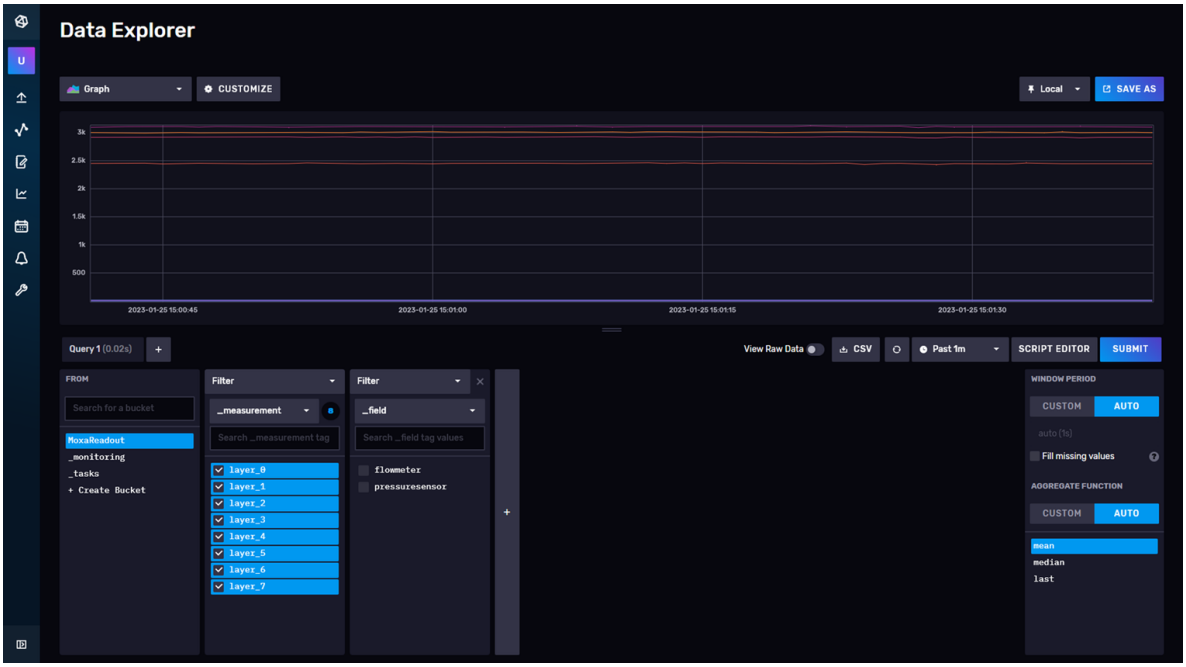

Figure 18: InfluxDB example of a eight graphs displayed simultaneously.

5.8.3 Grafana Interface

As the sensor interface, Grafana was chosen. Queries from InfluxDB can be directly copied into Grafana, allowing plotting of chosen data in a chosen graph, with chosen data processing method. Grafana interface allows for as many separate graphs as needed, these can be fully modified to fit the data. Graphs are easy to read and easy to work with.

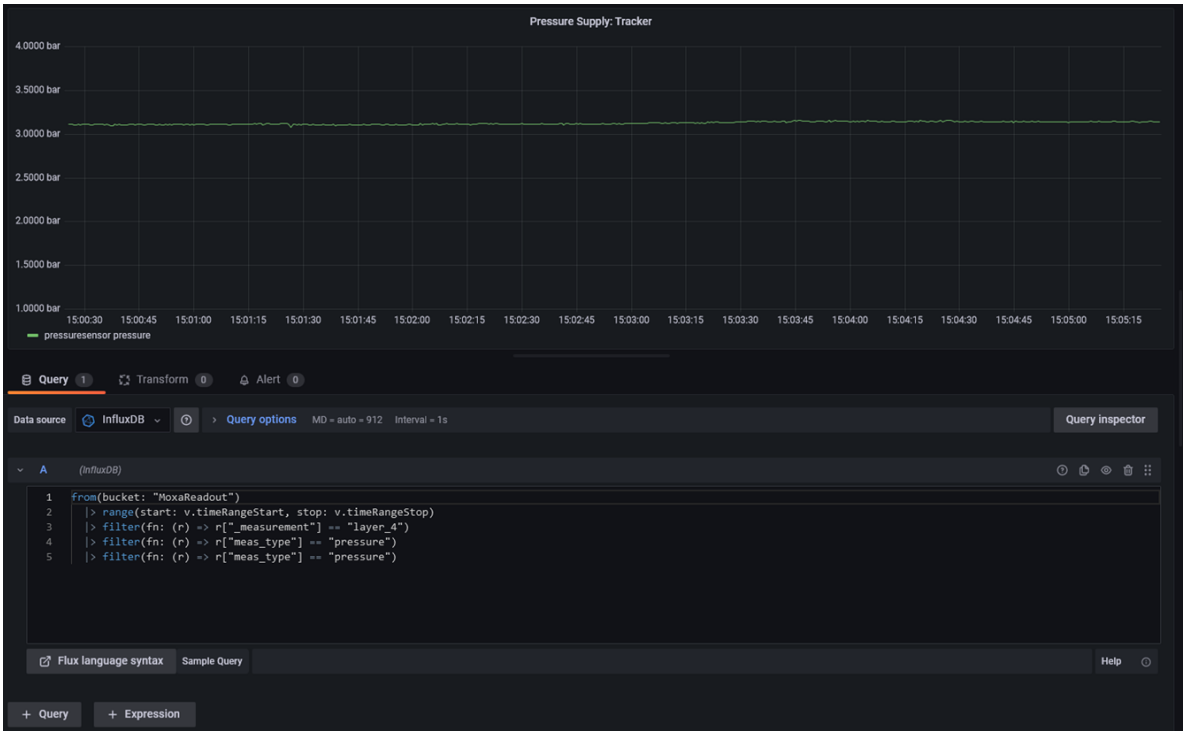

Figure 19: Queries can be copied directly from InfluxDB to Grafana. An example with the pressure sensor for Tracker water supply.

Figure 20: Grafana example of two separate graphs. Grafana allows for displaying data from any given sensor with chosen axis labels. Graphs can be organized on the same plot or separated at will.

6 Sensor Calibration and Validation Measurements

Before any tests on the cooling system were committed, some of the sensors required calibration as their calibration status were unknown. Most important were the flowmeters and the PT-1000 RTD sensors. The pressure sensors were already pre-calibrated and required no further inspection as their values still aligned with provided fitting curves. This chapter will describe the methods used for calibration, further outlining the results with some error analysis.

6.1 Sensor Calibration

The sensors required some validation of their calibration status'. While for this project, high precision of the sensors was not a priority, a measurement of deviation from the factory calibration was desirable, as characterizing the system with large offset could potentially make the results invalid. The pressure sensors have been calibrated before and flowmeter temperature sensors agreed mostly with the temperatures shown at the chiller, so no calibration was deemed necessary for both. The flowmeters were at first assumed to be as accurate as written in the data sheet provided. However, they have not been used in a while, so recalibration was desired to check their status. The RTD sensors were calibrated whenever necessary, reason is outlined in 6.3.

6.2 Flowmeter Calibration Setup

Method used for calibrating flowmeters is very simple. Since flow rate can be found simply by measuring the amount of liquid that collects during a given time, we simply pass water through the flowmeter, measure the amount and divide by the measurement time. Given by equation (15)

$$Q = \frac{V}{t} \tag{15}$$

The setup used consisted of a 10L bucket at the sensor output. The sensors were both connected to the chiller pump output using a splitter, this allowed for flow rate variation using the regulation valve of the chiller.

Per manufacturers datasheet [22], for nominal precision, see page 5, a straight pipe length of at least 10cm for both flowmeters would be required. The chiller has a minimum level of water at around 14.5 L, and a maximum level at 19 L. Going below minimum sounds an alarm and stops the pump. This put a limit on the amount of water that could be used and became very noticeable when looking at error bars, especially at high flow rates.

Water in the chiller tank is de-ionized and treated with a solution of Sodium 2-ethylhexanoate provided by the chiller manufacturer at a ratio of 40:1. It's a preventative measure for any algae growth and sediment forming. The density of the added solution was negligibly larger than that of freshwater, at 1.007 g/cm^3.

6.2.1 Measurement Procedure

The measurement process was very straightforward. The chosen sensor was opened and the other closed. Then the pump regulation valve was manually opened by hand, starting the measurement. Data was read every 0.5 s, and plotted live, in addition to being stored in a text file for review. The water is collected in a bucket with known weight, thus weighting it after measurement reveals how much water passed through the sensors. Each data point in figure 21 and figure 22 is an average of all measured flow rates during the time it took the pump to drain the tank from maximum to minimum level.

6.2.2 Calculation Error

Naturally, since the mean of the values is taken, an error proportional to measurement time will be introduced. This error grows significantly larger the fewer measurement points there is, or in other words, the higher the flow rate is. Opening the valve takes a brief moment, and then it takes another moment for the flow to reach its stable value. This means between 1-3 measurements at the start and the end, in any series, will be a lot lower than expected. Looking at figure 21 in Calibration Results, when the flow rate is high with only 20 measurement points total, having even two of these that deviate strongly will cause a very large standard deviation. This is the main cause of errors in current measurements, along the x-axis.

Flow rate measurements errors, along the y-axis, stem mainly from time and weight uncertainty. For time measurement, an uncertainty of ±2 s was assumed due to time resolution of readout being 0.5 s at the start and at the end. In reality, it is a little more than 0.5 s so ±1 s uncertainty would not be sufficient. Scale uncertainty was ±1 g for the whole range. However, the scale was never calibrated, and the bucket was never dried between each measurement leaving residual water in it. Therefore, the uncertainty in weight measurement was assumed to be ±50 g. This flat weight uncertainty also encompassed the fact that water in the chiller had additives, and that for ease of calculation it was assumed that 1 g of weight in bucket equaled 1mL of water when calculating flow rate. Even so, weight uncertainty was mostly insignificant in comparison to time uncertainty.

6.2.3 Calibration Results

Calibration of PF3W520S and PF3W504S can be seen in figure 21 and figure 22 below. These graphs show two plots, one for the ideal linear relation called "Ideal", and one obtained from measuring and linearly regressing data points called "Measured". For this procedure, due to time constraints, repeatability of measurements was not considered, due to the difficulties of precisely operating the chiller valve. In hindsight, measuring this property inaccurately would be better than not measuring it at all, as the calibration result would be more trustworthy. For PF3W520S the flow rates below 5 L/min can't be considered to have good repeatability, as seen by the two points at 4 L/min above the "Ideal" line. For same reason, this calibration can't be concluded to be valid for flow rates below 6 L/min. For PF3W504S all the results lie below the "Ideal" line. This results indicate there was deviation along the whole flow meter range.

One interesting point is the one representing the maximum chiller pump output. The rightmost point in figure 21 with a value of 15.15 ± 0.88 L/min. Comparing this to the sum of flows through the tracker and the calorimeter, 3.36 ± 0.10 L/min + 12.05 ± 0.36 L/min = 15.41 ± 0.37 L/min. From these two results we can conclude that the chiller pump has higher flow output than the value in manufacturers data sheet [23].

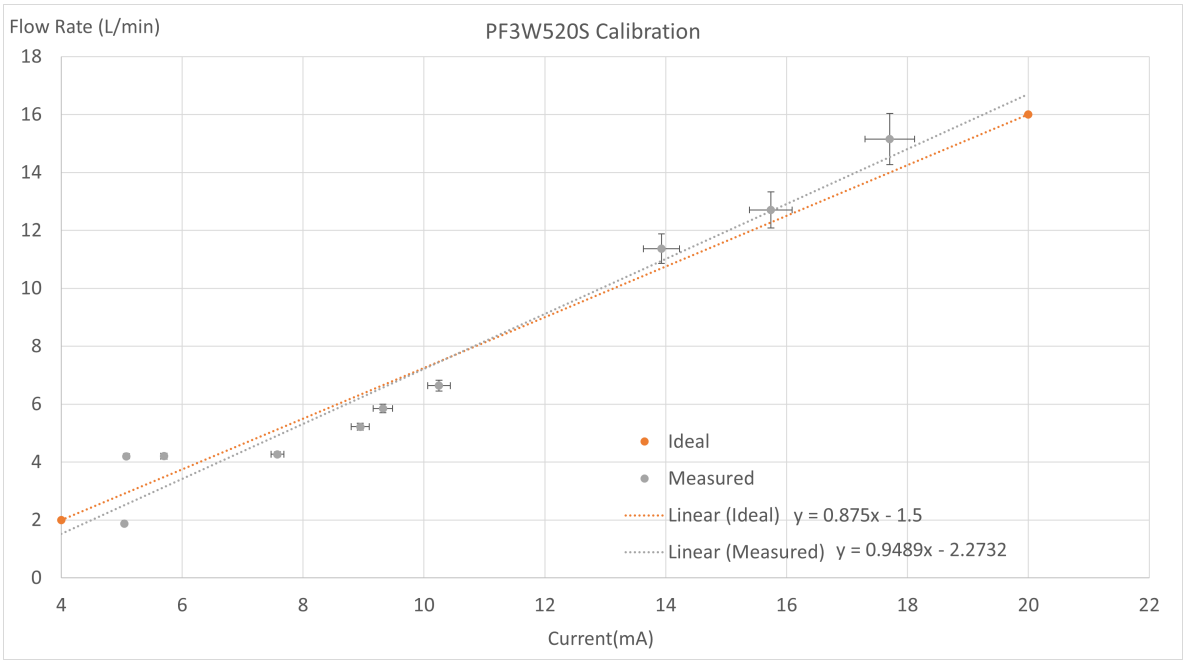

Figure 21: Calibration graph of PF3W520S Flowmeter, plotted together with ideal linear output of the flowmeter.

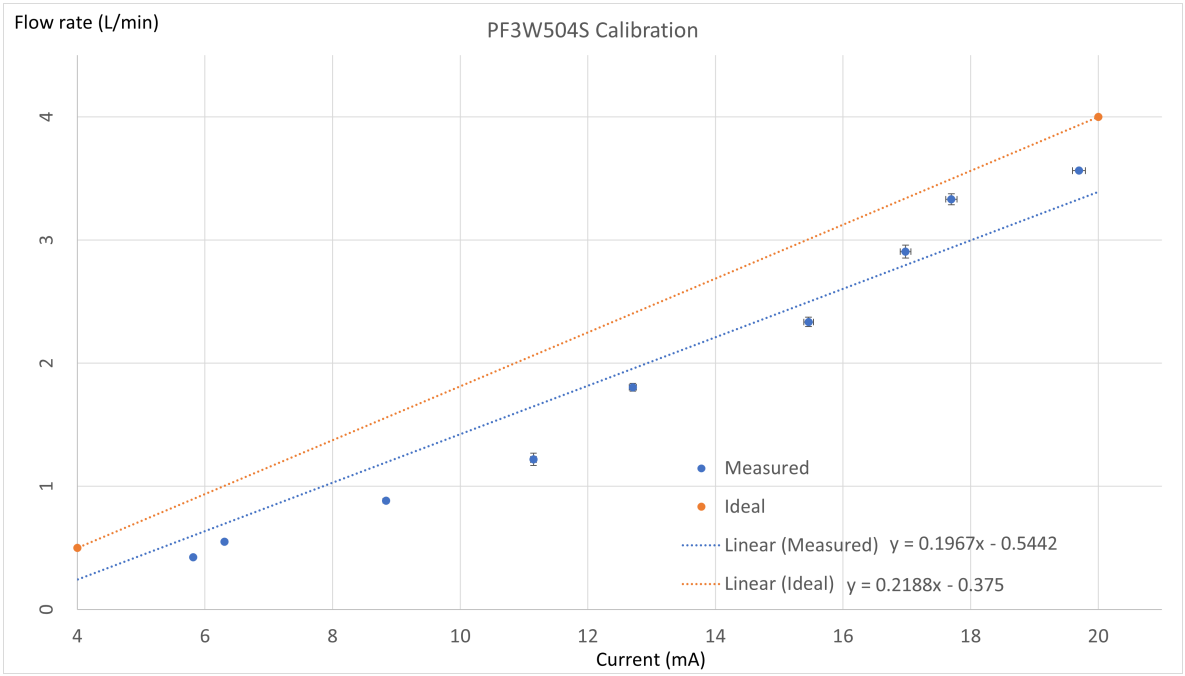

Figure 22: Calibration graph of PF3W504S Flowmeter, plotted together with ideal linear output of the flowmeter.

6.3 Calibrating of the PT-1000 Sensors

The PT-1000 sensors were calibrated once so they display equal values. The MOXA E1260 has an inbuilt calibration function, which was used to calibrate the sensors in an ice bath. After this procedure, the Moxa was turned on/off once with the sensors still in the ice bath, to see if the calibration persisted as it should.

However, due to a behavior of the MOXA E1260 module, which manifested itself as the sensors sometimes recalibrating or jumping between extreme values, the PT-1000 sensors were to be calibrated whenever there was a suspicion that this behavior distorted the measurements. This was repeated a total of nine times over a period of the first two weeks of use. This behavior seemed to have been caused by repeated use of inbuilt MOXA calibration option, in quick successions in the span of less than one minute, which had to be done due to poorly made ice bath. The problem ceased to appear whenever the sensors were calibrated only once every five minutes. The required wait time before calibrating again was not precisely pinpointed, therefore whenever calibration is required it is recommended to only do once, but thoroughly.

6.4 Measurement of Flow Rate with Respect to Pressure

Measurements of flow rate with respect to pressure help with two things, while also validating the calibrated sensor output. First it allows for calculation of the mechanical power of the coolant using flow rate and return pressure, and second it gives insight into resistance of the system. Resistance in this case is the relation between increase in pressure and the corresponding increase in flow rate. The higher the resistance the less flow increases with each increase in pressure, seen by flattening of the curve in figure 23 and figure 24. This representation is only qualitative, the quantitative calculation of resistance was not part of this work. Data is given in tables 5 and 6 and plotted in figure 23 and figure 24, for tracker and calorimeter respectively.

Table 5: Table of measured return flow rate, supply pressure and return pressure. For the tracker.

Flow Rate (L/min)	**Supply (bar)**	**Return (bar)**
3.9	3.36	3.24
3.28	2.69	2.61
2.66	2.13	2.08
2.02	1.67	1.64
1.28	1.30	1.28
0.7	1.14	1.14

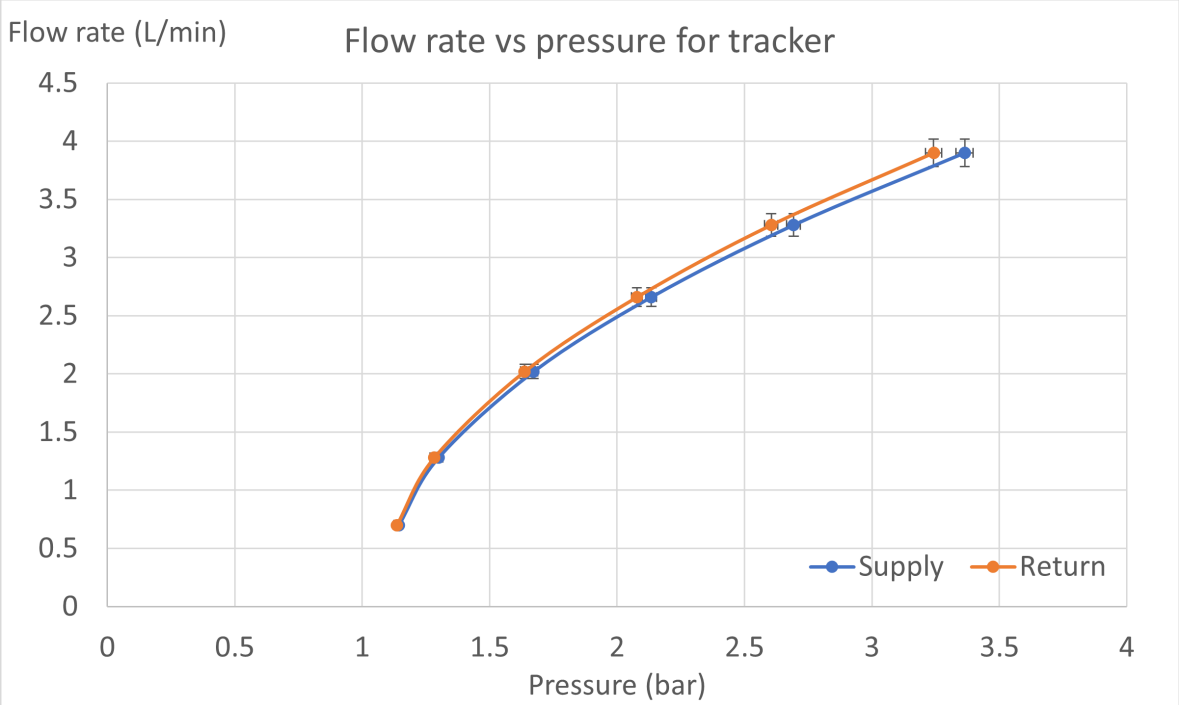

Figure 23: Flow rate with respect to pressure for the tracker. It shows both the pressure drop and resistance in the system.

Table 6: Table of measured return flow rate, supply pressure and return pressure. For the calorimeter.

Flow Rate (L/min)	**Supply (bar)**	**Return (bar)**
11.8	3.14	2.62
10.8	2.79	2.36
9.37	2.34	2.02
7.96	1.95	1.73
6.0	1.54	1.42
4.33	1.29	1.23
3.38	1.18	1.15

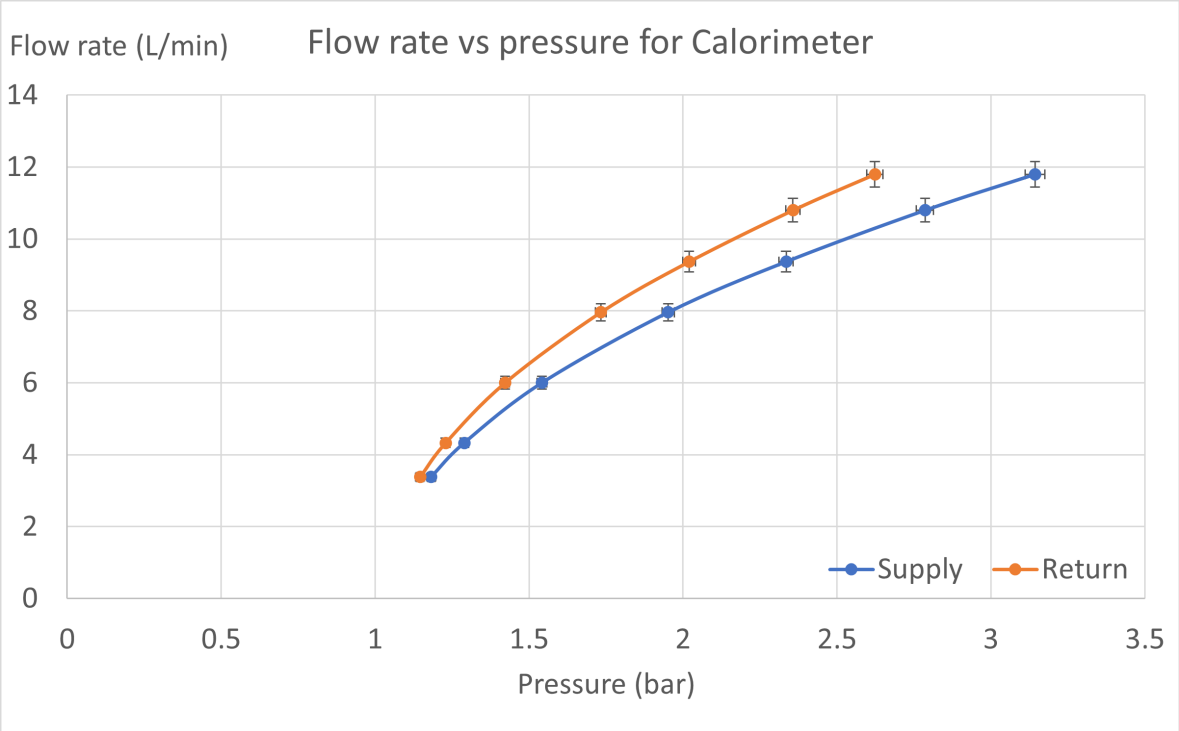

Figure 24: Flow rate with respect to pressure for the calorimeter. It shows both the pressure drop and resistance in the system.

7 Cooling System Testing

This chapter will explain various tests which would allow to make predictions on performance of cooling system in the final prototype. As well as that various other properties were examined, like thermal stabilization time and long term performance.

7.1 General Testing Environment and Considerations

Unless specified, the room temperature varied between 22.5 °C (before powering) to 25 °C (after thermal stabilization) for all the tests. There are two main reasons, heat up due to the DTC and chiller running, as well as variations in air draft temperature through the lab. As well as that, the chiller setpoint temperature was set to 18°C by default.

One important aspect to consider is the mass of the DTC, so the measurement shouldn't be taken before it is thermally equalized with the environment, this is mainly important when measuring temperatures at the calorimeter. This thermal stabilization, for the calorimeter, takes 1.5 hr±15 min, depending on power to pads and coolant flow through the system. The tracker takes around 15±3 min to thermally stabilize, depending on power and coolant flow rate.

7.2 The Chilling Cycle

The chiller doesn't keep coolant temperature perfectly at the setpoint. What actually happens is that the chiller doesn't start chilling before the coolant temperature reaches exactly 2.1 °C above the setpoint. Once it does, the unit activates and runs until the temperature drops exactly to the setpoint. However, due to some small residual cooling, the temperatures will drop between 0.3-0.4 °C below the setpoint. This cycle is what is referred to as the chilling cycle.

7.3 The Plateau Condition

An important thing to mention is the idea of plateau condition. Since the lab is not a climate chamber, there is no simple way of controlling the air temperature or air

flow inside it. As well as that the issue of environment heat up has to be considered. This means the temperatures will to some degree always be changing, either increasing or decreasing. Therefore, a stopping condition, called the plateau condition, was introduced. This condition is simple, whenever temperature changes insignificantly in any given amount of time, the temperature is measured at that point. Since the temperature will be oscillating, as caused by the chiller, the temperature will always be measured at the peak of this cycle, and the stopping condition will be considered by looking at changes in those peaks.

Generally, this condition was set to be a change of temperature dT = 0.1 °C/5 min for the calorimeter, and dT = 0.2 °C/min for the tracker. The large difference stems from mass to surface area ratio, with calorimeter being less affected by changes to the environment.

7.4 Checking Temperatures at Various Heating Sources' Powers with Constant Flow Rate

The first test consisted of checking temperatures while varying the heating sources' power. For this purpose, heating pads in the calorimeter and heating strips in the tracker were used. The reasoning is simple. Since we have expected energy usage of the ALPIDEs, we have an idea of the amount of heat generated that needs to be removed. This heat can be then emulated using these heating sources. This method wasn't about precisely reproducing the heat distribution in the DTC as, especially in the calorimeter, emulating the ALPIDEs and the absorbers would be too time consuming and rather difficult due to space limitations. The spots chosen for the calorimeter and the tracker were discussed in 5.5. The procedure itself consisted of keeping the flow at maximum value for both the tracker, 3.9 L/min, and the calorimeter, 11.9 L/min, and decreasing power from the heating element from maximum power, 1000 W for the calorimeter and 22 W for the tracker, to minimum in five equal steps, see table 7. Doing it from the top down to the bottom allows for faster thermal stabilization.

A situation without cooling was repeated to assess how quickly the system reaches critical temperatures, and what equilibrium temperatures were for various power levels. This also shows temperature difference for case of cooling and no cooling.

Table 7: Table of used electrical power to the heating elements for the calorimeter and the tracker. Due to a power miscalculation to the calorimeter the table presents intended values for power, and actual values with miscalculation corrected.

Intended electrical power (W) to the calorimeter heating elements	1000	800	600	400	200
Actual values (W) for the calorimeter	985	644	363	161	42
Electrical power (W) to the tracker heating elements	22	17.6	13.2	8.8	4.4

7.4.1 The Tracker Results

The results of the tracker temperatures measurements with respect to heating sources' power in three cases. The tracker temps were measured for cases with water and air cooling, no cooling, water only cooling and air cooling only.

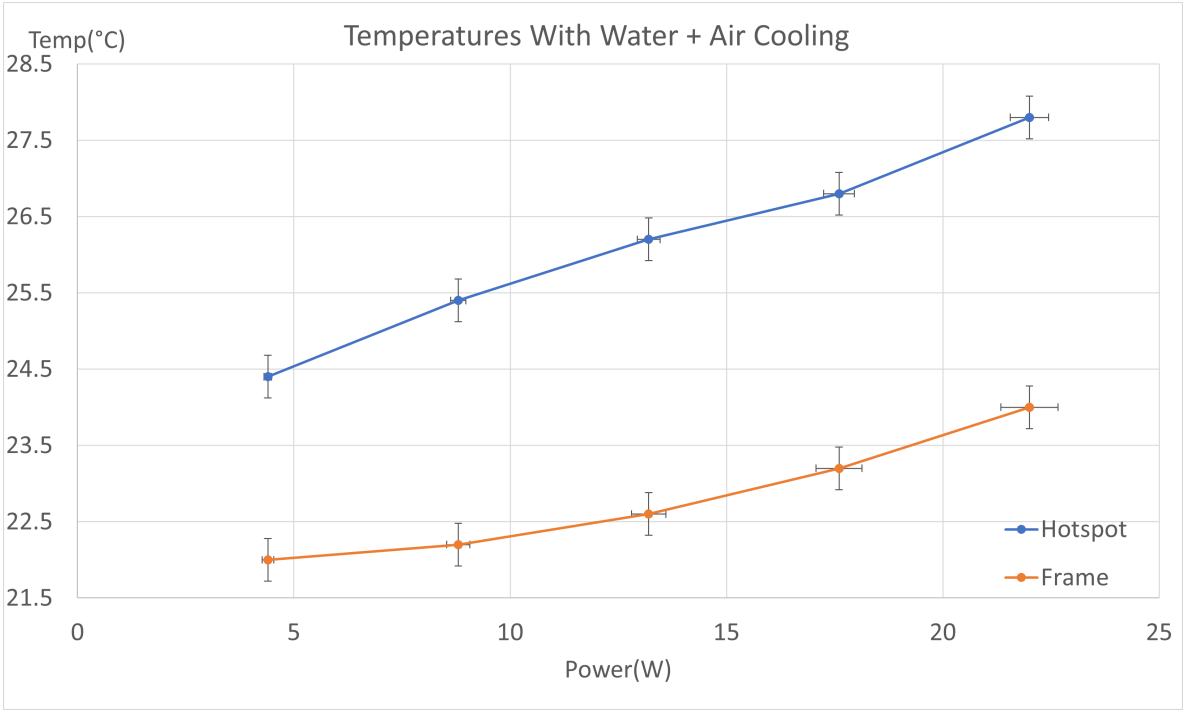

Figure 25: Tracker temperatures at hotspot and frame, air and water cooling.

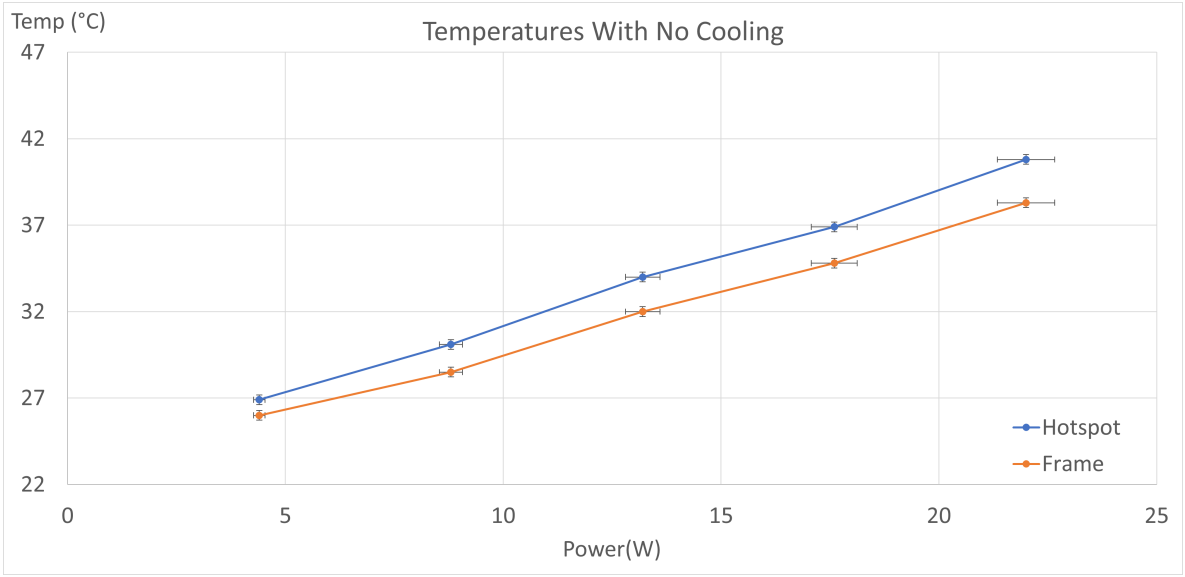

Figure 26: Tracker temperatures at hotspot and frame, no cooling.

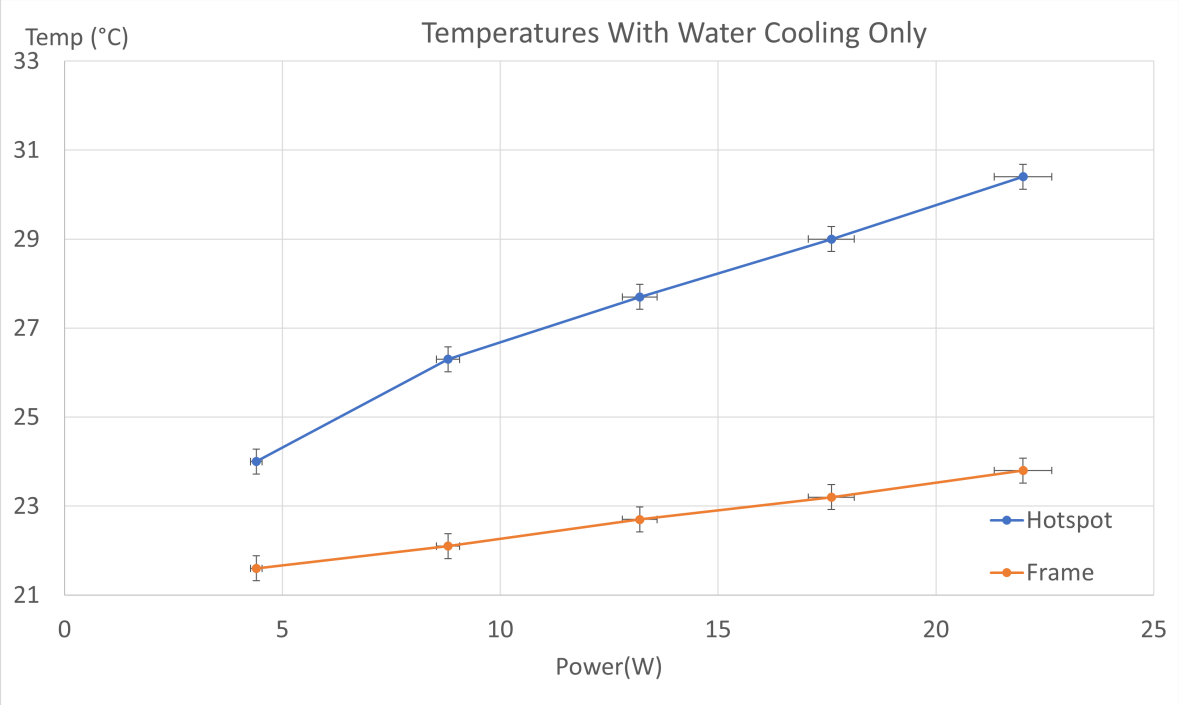

Figure 27: Tracker temperatures at hotspot and frame, water cooling.

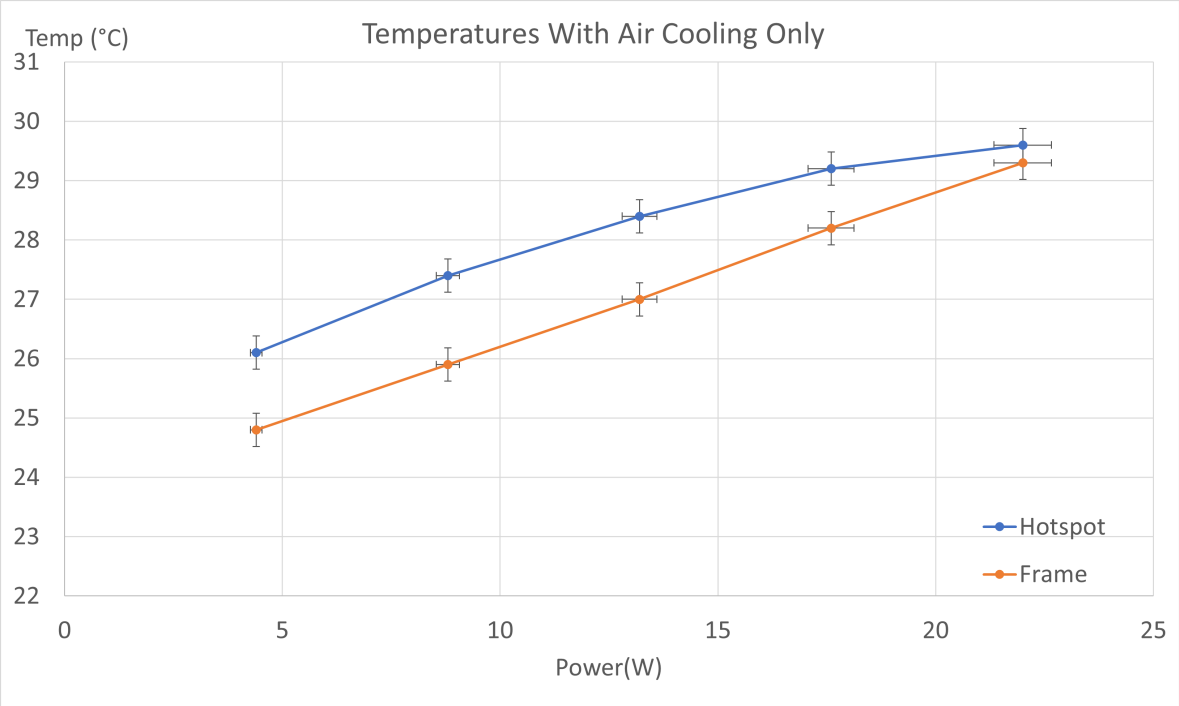

Figure 28: Tracker temperatures at hotspot and frame, air cooling.

Thermal image shows temperature distributions across the tracker layer with the current distribution of heating elements. Note that there is a paper sheet in front of

tracker as to reduce reflection allowing capturing thermal images. However, this paper sheet was at a later time noticed to not be fully in contact with the heating elements, making the heat distribution a little different than the expected elliptical distribution.

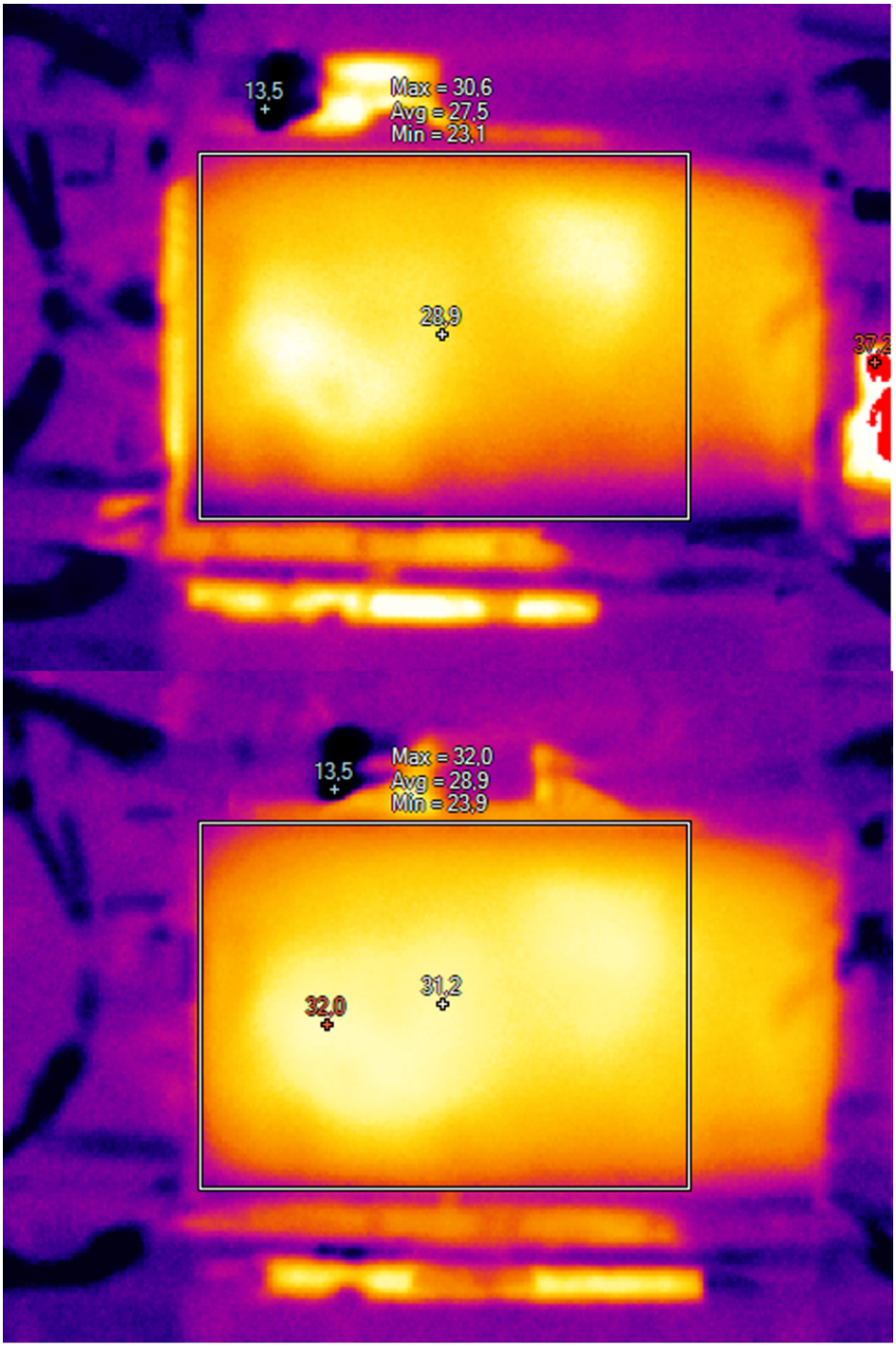

Figure 29: Thermal images of the tracker. Top one shows heat distribution with water and air cooling. Bottom one shows heat distribution for water cooling only.

7.4.2 Calorimeter Results

Calorimeter results are shown in figures 30 and 31 below, for measurements with and without cooling.

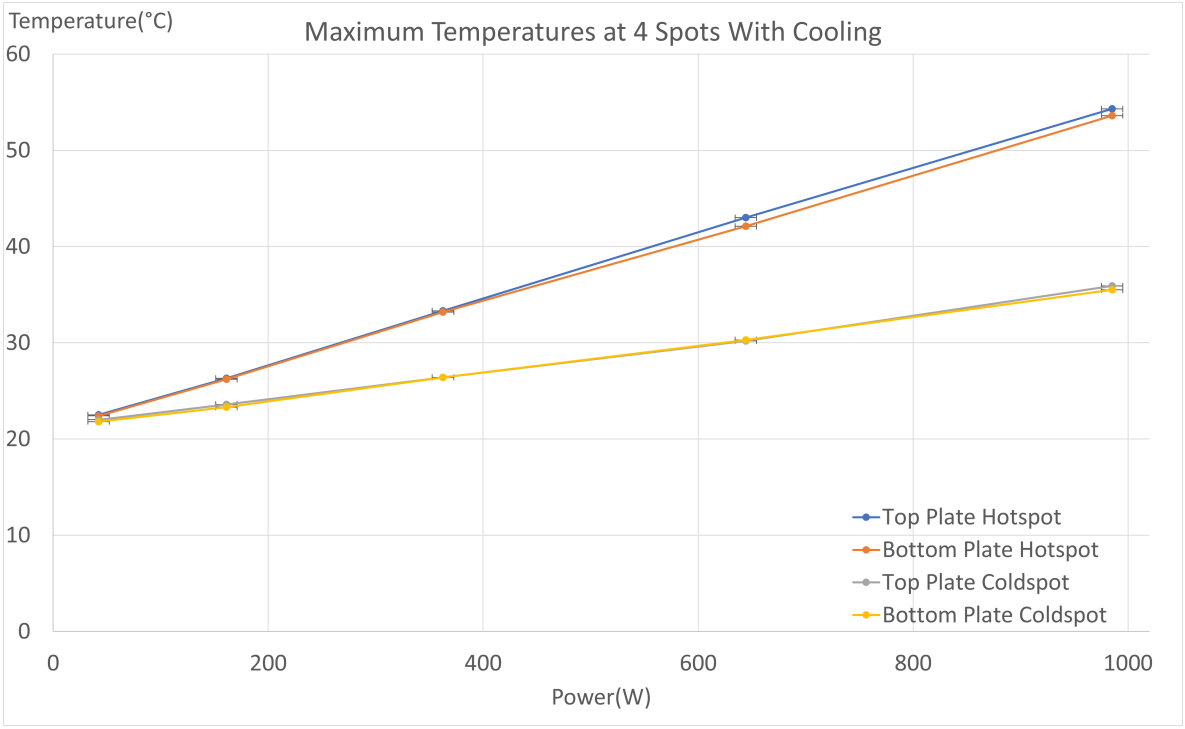

Figure 30: Temperature results from the calorimeter hotspot and coldspot at various power levels with water cooling at maximum performance.

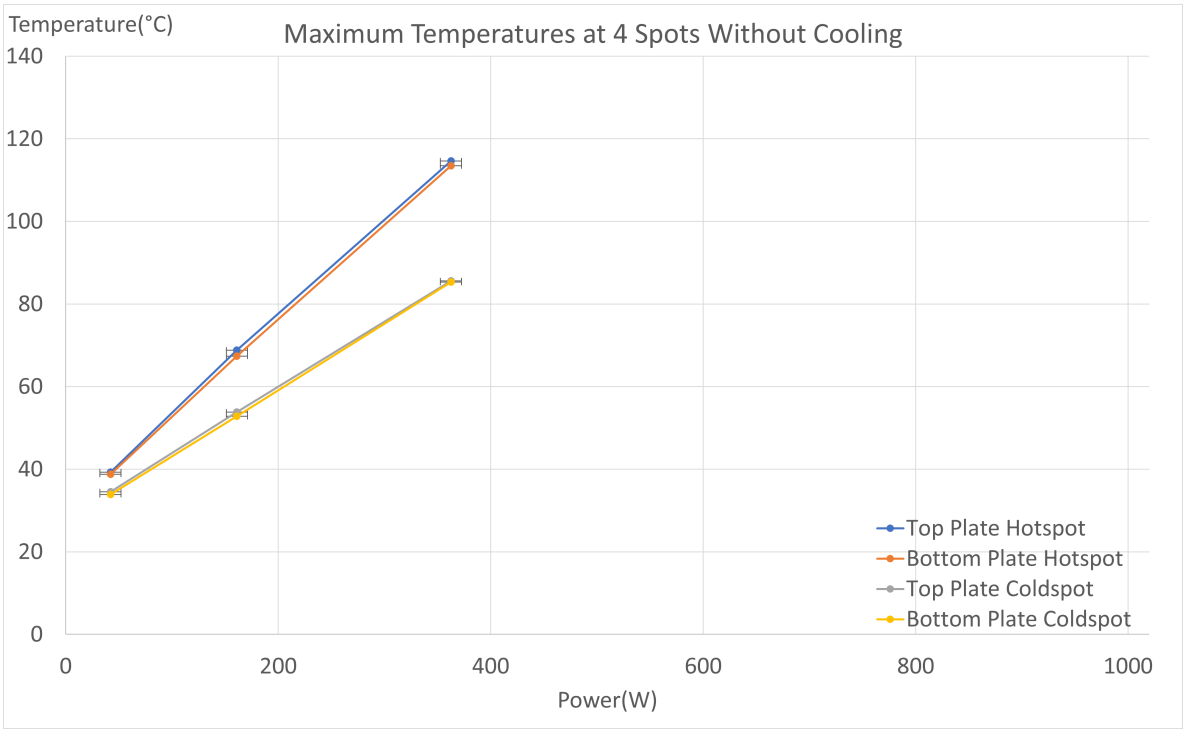

Figure 31: Temperature results from the calorimeter hotspot and coldspot at various power levels with no cooling. No data beyond third point due to high temperatures.

7.5 Checking Temperatures at Various Flow Rates with Constant Power

Measuring temperatures at various flow rates in the tracker and the calorimeter allows for characterization of water cooling performance. Generally, we want to avoid running the cooling system at 100% of its performance due to wear build-up. Performance being defined as percentage of maximum cooling system output, in this case only water cooling is considered as air cooling was not analyzed in depth. Performance of the water cooling was investigated at 80% performance and at 60% performance, and gives a good indicator of how much the flow rate can be reduced without a significant temperature increase.

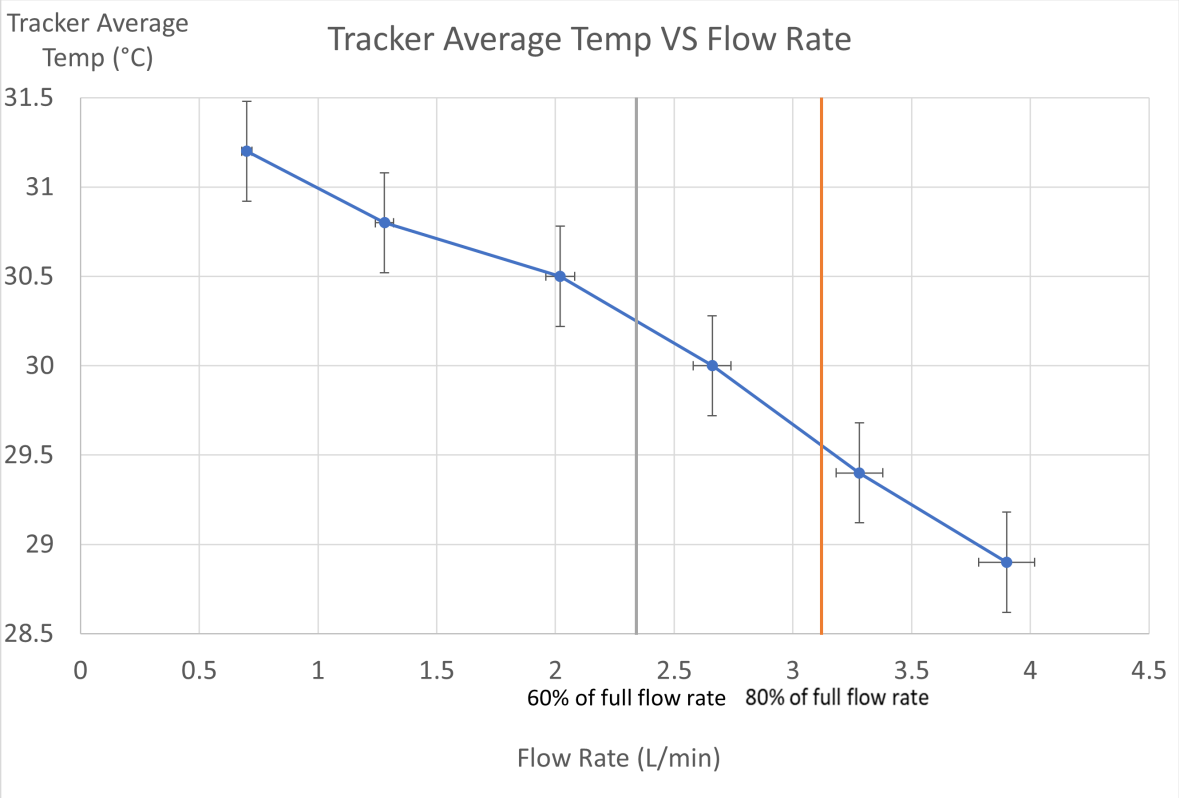

Figure 32: Graph showing average temperature of the tracker with respect to flow rate, temperatures measured using a thermal imager. Vertical lines represent points of 80% and 60% performance. Water cooling only.

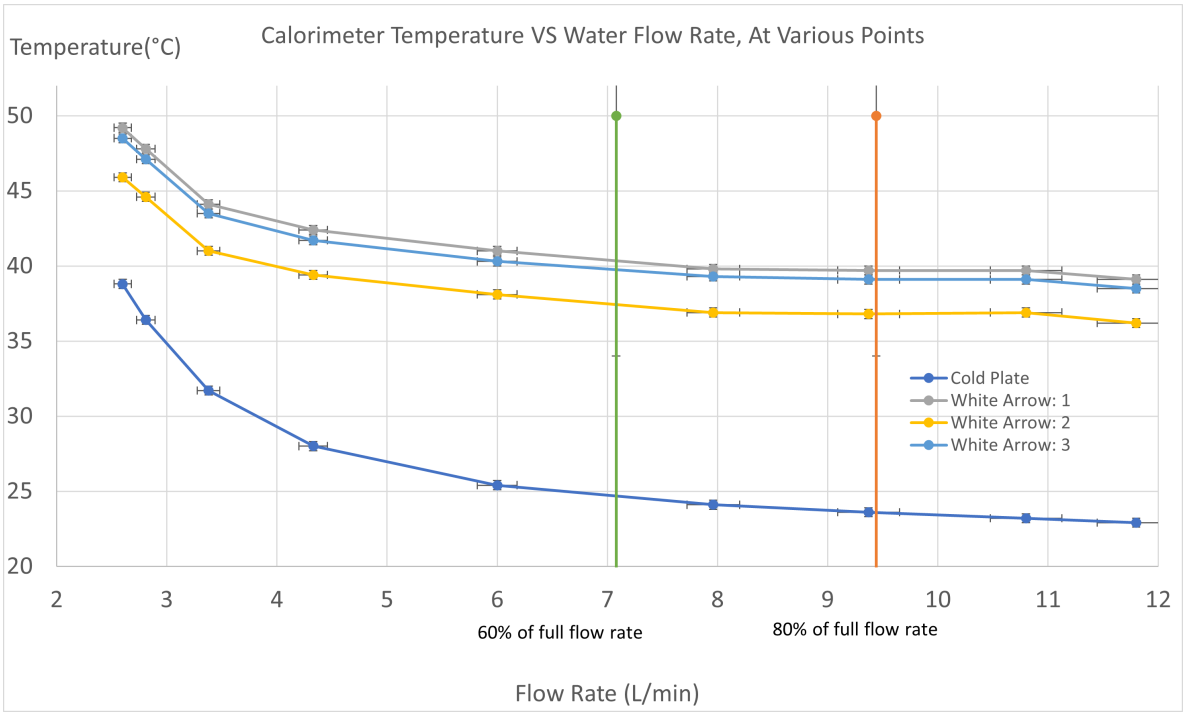

Figure 33: Graphs showing temperatures at cold plate center and points seen in 13 with respect to flow rate. Vertical lines represent points of 80% and 60% performance.

7.6 Checking Change in Coolant Temperature

Measuring change in coolant temperature between inlet and outlet allows for calculation of heat absorbed by it. This value can then be compared to the total power inserted into the system, giving information on quality of measurement or if all important power sources and drains were considered.

Now, the average change in water temperature will be measured, it is measured over two chilling cycles, so roughly 30 minutes of time. The main reason is that measuring at a single point in the cycle doesn't really tell us that much, as the temperature differences are larger right at start of the cycle and smaller at the end. So, taking one measurement point could yield either a high or low temperature difference.

The results are put into table 8. Having them in a single table allows for quick look up of how ΔT changes with flow rate in the tracker and the calorimeter, useful when adjusting the flowmeter valves.

Table 8: The results from measurement in ΔT of water, between inlet and outlet, for the two tracker tubes and the two calorimeter cooling plates.

Tracker flow rate (L/min)	**Tracker change in water temperature between inlet and outlet (°C)**	**Calorimeter flow rate (L/min)**	**Calorimeter change in water temperature between inlet and outlet (°C)**
3.90	0.30	11.90	1.97
3.28	0.82	10.80	2.09
2.66	1.19	9.37	2.56
2.02	1.84	7.96	3.09
1.28	2.71	6.00	4.36
0.70	3.27	4.33	6.90
-	-	3.38	10.94

7.6.1 Change in Coolant Temperature in Tracker

The water temperature were measured at top and bottom water inlet and outlet, giving a total of four points in pairs, see chapter 5.5.1. The power was kept at nominal value of 22 W for the tracker meanwhile the flow rate was changed at six roughly equal steps with no air flow:

Flowrate(L/min)	0.7	1.28	2.02	2.66	3.26	3.9

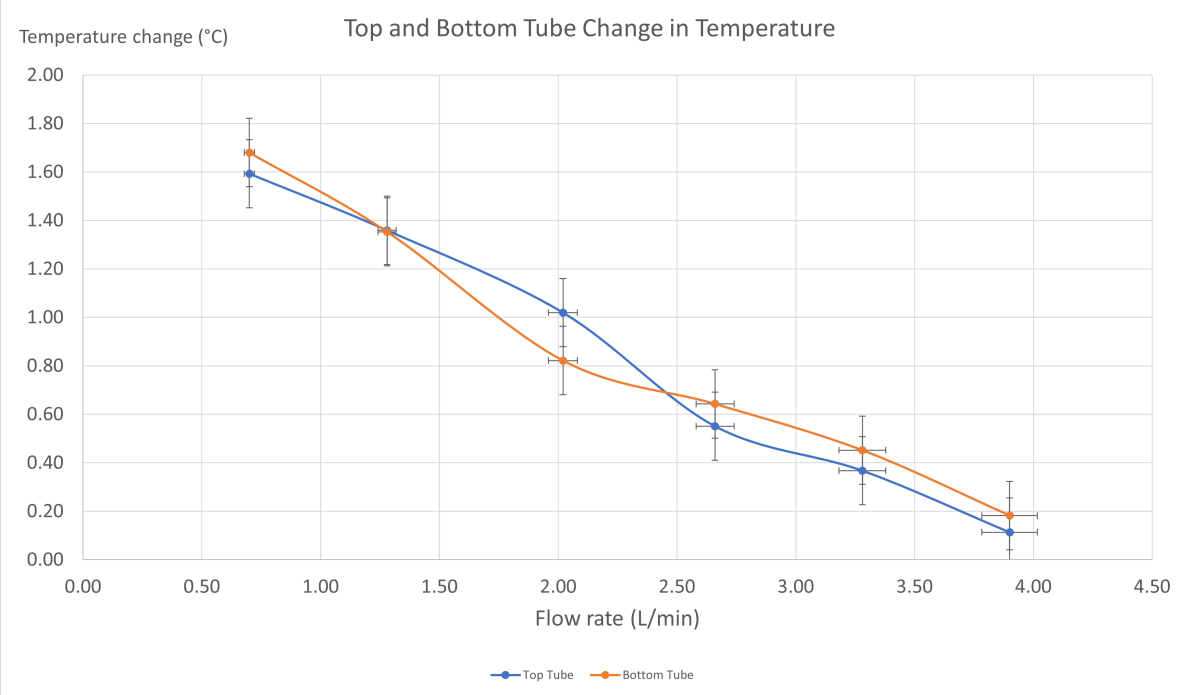

Figure 34: Tracker change in water temperature between inlet and outlet in a single layer bottom tube and top tube.

7.6.2 Change in Coolant Temperature in Calorimeter at Constant Power and Varying Flow Rate

Water temperatures was measured at inlets and outlets to the calorimeter cooling plates, pairwise. This gives four measurement points, as seen in figure 10. While the power was kept at value of 815 W, originally intended to be the ALPIDE nominal power consumption of 896 W, but power was miscalculated in the same way as table 7 for the calorimeter meanwhile the flowrate was changed at six roughly equal steps:

Flowrate(L/min)	3.38	4.33	6.00	7.96	9.37	10.8	11.8

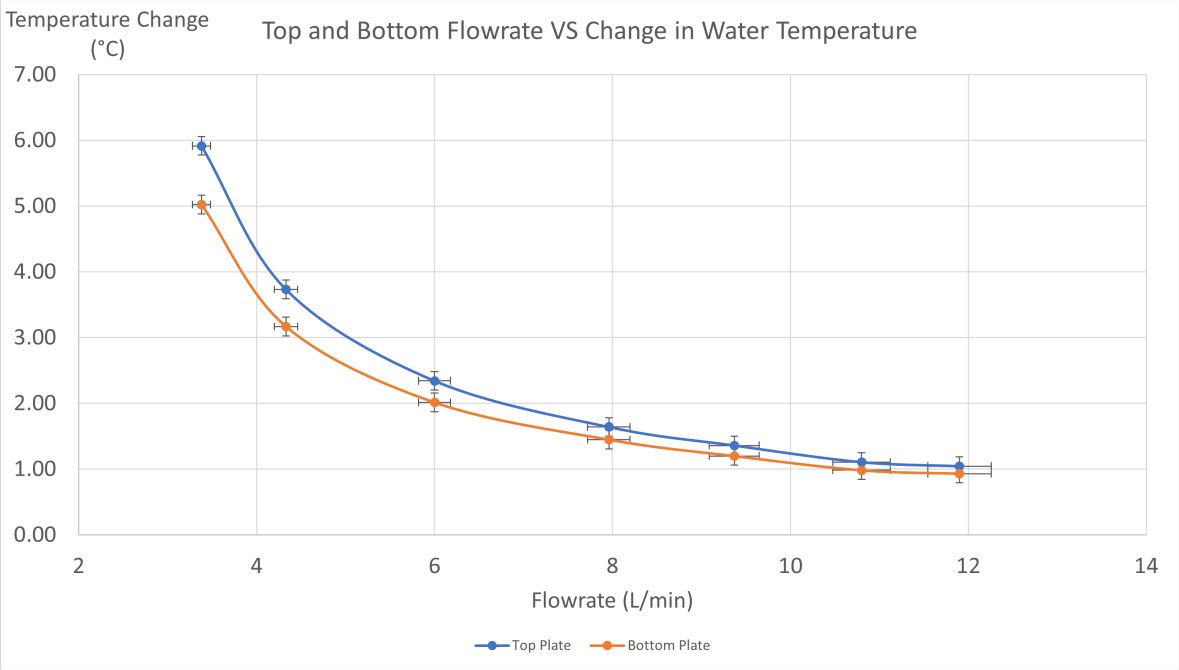

Figure 35: Calorimeter change in water temperature between inlet and outlet at bottom plate and top plate.

7.7 Air Temperature Inside the Calorimeter with Changing Chiller Setpoint

The idea behind measuring the temperature of air inside the calorimeter was to emulate the final detector design and look at how temperature behaves with changing chiller setpoint with constant power and constant cooling, expected linear. Since the whole calorimeter will be mostly filled, with little to no free space, measuring the temperatures inside the dummy chamber we have now without allowing air exchange would allow to emulate how hot this chamber would get in the final design.

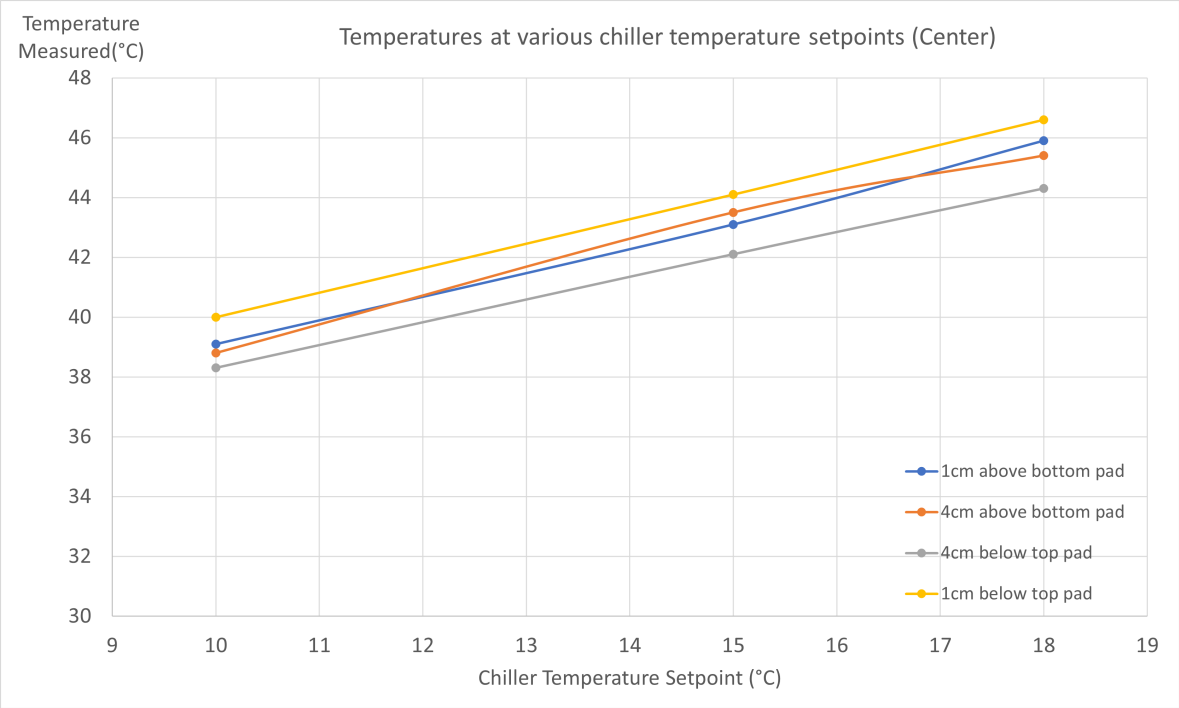

Figure 36: Air temperature with respect to chiller setpoint temperature at "Center" spot for the chiller.

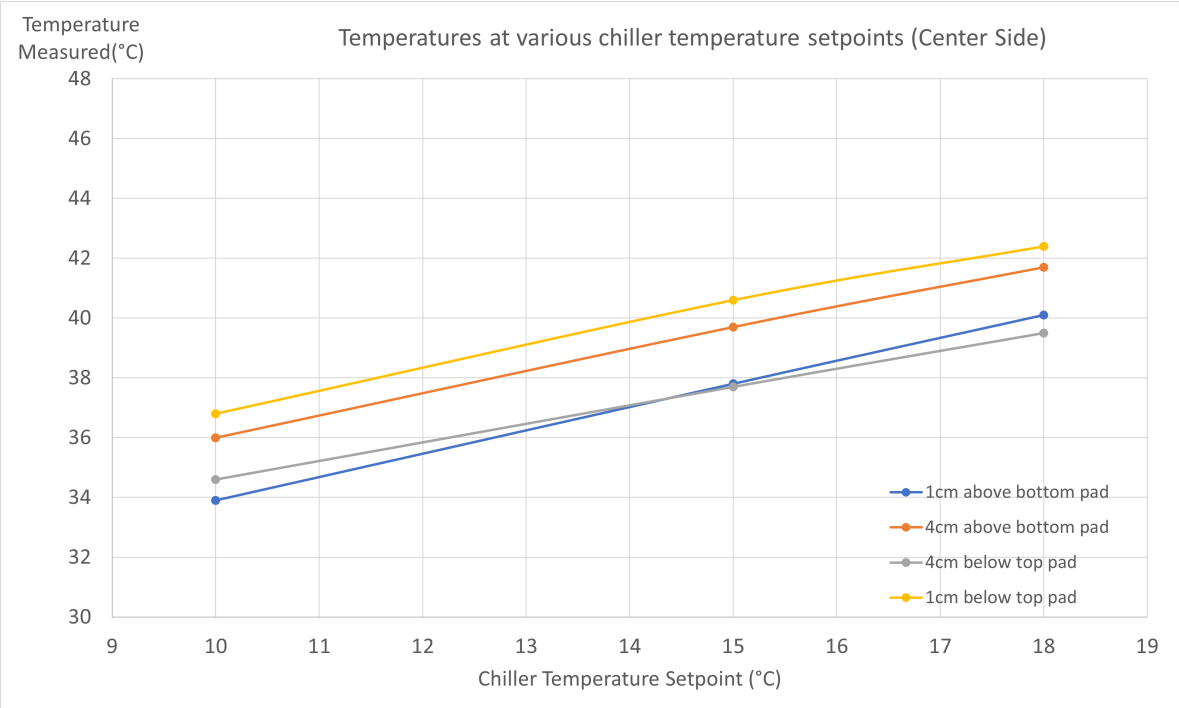

Figure 37: Air temperature with respect chiller setpoint temperature at "Center Side" spot for the chiller.

8 Result Discussion and Conclusions

This chapter will discuss results of the tests, how accurate they are in the context of the prior works and simulations. As well as that some outlook on the future of the project will be given.

8.1 Tracker Results Discussion

The tracker, rather unsurprisingly, managed to stay within reasonable temperatures for all heating powers and cooling combinations. The electrical power supplied is low for a large area and small thermal capacity which means it quickly heats up. However, this also manifests itself as non-linear temperature behavior, as seen in figure 25, 26, 27 and 28. This non-linearity was likely caused by how easily the tracker is affected by the environment. As an example, someone walking by disturbing air in the laboratory.

The main difference between only using water or air cooling is the temperature at the frame, which is an expected result as the frame is massive with a small surface area, compared to the tracking layer itself. Air cooling is highly dependent on ambient temperature and is believed to have higher efficacy at lower ambient temperatures than the ones at the laboratory. Looking at result without cooling 26, we can expect to stay within the ALPIDE temperature limit even for values of power reaching nominal value of 22 W. This is however believed to be slightly incorrect. Later in testing it was discovered that the tracker layer without cooling, given enough time, could reach slightly higher temperatures, this was likely caused by the standing water in the water cooling tubes serving as a heat reservoir, essentially slowly soaking the heat from the tracker layer. In addition, the plateau condition was, most certainly, too lax in this case. However, quantifying this is highly unlikely to yield any useful information as the system is not expected to run without cooling.

8.1.1 Heat Removed by Water in the Tracker

From results in figure 34, it is possible to calculate the heat absorbed by water, with values and uncertainties visible in table 9 and plotted on figure 38. As mentioned in chapter 3.9, the flow is assumed to split evenly between all the tubes, as they are in

parallel. So, the Flow rate through each tube in table 9 is the total flow rate divided by four, as there are four tubes.

Table 9: Measured change in temperature between inlet and outlet, in top and bottom tube. From that the calculated heat absorbed by water with uncertainties is presented.

Flow rate (L/min)	**Average ΔT over 2 chilling cycles in top tube (°C)**	**Average ΔT over 2 chilling cycles in bottom tube (°C)**	**Energy absorbed, top tube (W)**	**Energy absorbed, bottom tube (W)**
3.90±0.12	0.11±0.14	0.18±0.14	7.69±18.20	12.38±18.18
3.28±0.10	0.37±0.14	0.45±0.14	21.01±15.38	25.81±15.36
2.66±0.08	0.55±0.14	0.64±0.14	25.54±12.52	29.79±12.51
2.04±0.06	1.02±0.14	0.82±0.14	25.90±9.60	28.93±9.54
1.28±0.04	1.36±0.14	1.35±0.14	30.36±6.16	30.18±6.13
0.70±0.02	1.59±0.14	1.68±0.14	19.43±3.43	20.50±3.41

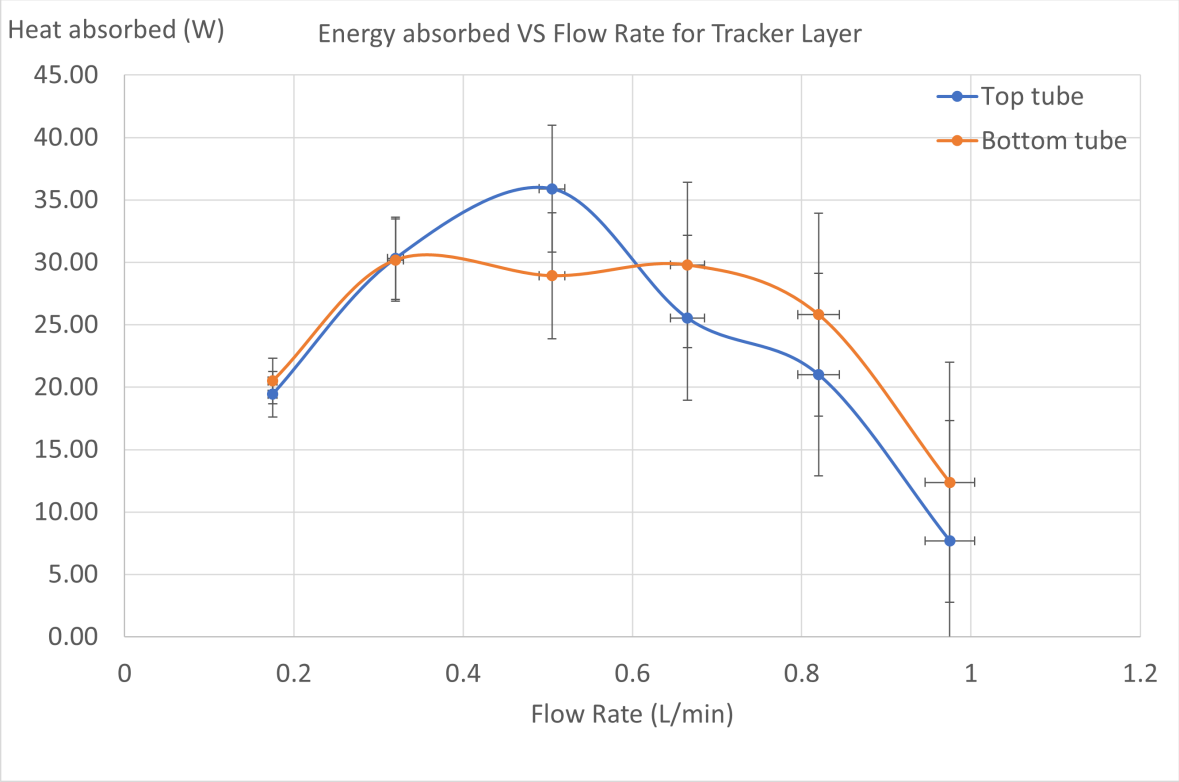

Figure 38: Heat absorbed by water in top and bottom tube in a single layer in the tracker.

Figure 38 shows a very clear transition between flow types. Laminar flow causing worse heat transfer for low flow rates, up to 0.5 L/min. The transitional flow in the middle likely causing the strange behavior in heat transfer between 0.5-0.7 L/min and turbulent flow for flow rates above 0.7 L/min. Compared to results in table 10 below, there are major disrepancies, meaning this qualitative analysis from the plot might not be correct. However, the value in that table come from a very simplified system, likely much higher due to complexity of the total tubing, seen in figure 5. Looking at calculated Reynold's number for figure 38 we get:

Table 10: Flow rate through each tube in the tracker and its corresponding Reynold's number.

Flow rate (L/min)	0.18	0.32	0.51	0.67	0.82	0.98
Reynold's number	423	752	1198	1574	1927	2303

These values for energy absorbed by water in each tube, found in table 9 can then

be used to calculate the total energy in table 11.

Table 11: Calculated total power in the system, as given in chapter 3. Q_L is the sum energy absorbed by water in top and bottom cooling tube in the tracker, with values found in table 9. Uncertainties of P_E, P_M, Q_C << uncertainty of Q_L, in the order of 1 to 100 and are therefore ignored for simplicity, see chapter 3.5.

Flow Rate (L/min)	Q_L**(W)**	P_E**(W)**	P_M**(W)**	Q_C**(W)**	**Missing Power (W)**
3.90	20.07±13.61	22	10.54	6.46	-6.01±13.61
3.28	46.82±11.48	22	7.12	6.96	24.66±11.48
2.66	55.33±9.35	22	4.61	7.56	36.28±9.35
2.02	64.82±7.18	22	2.76	8.06	48.12±7.18
1.28	60.5±4.64	22	1.37	8.36	45.49±4.64
0.36	39.93±2.58	22	0.66	8.76	26.03±2.58

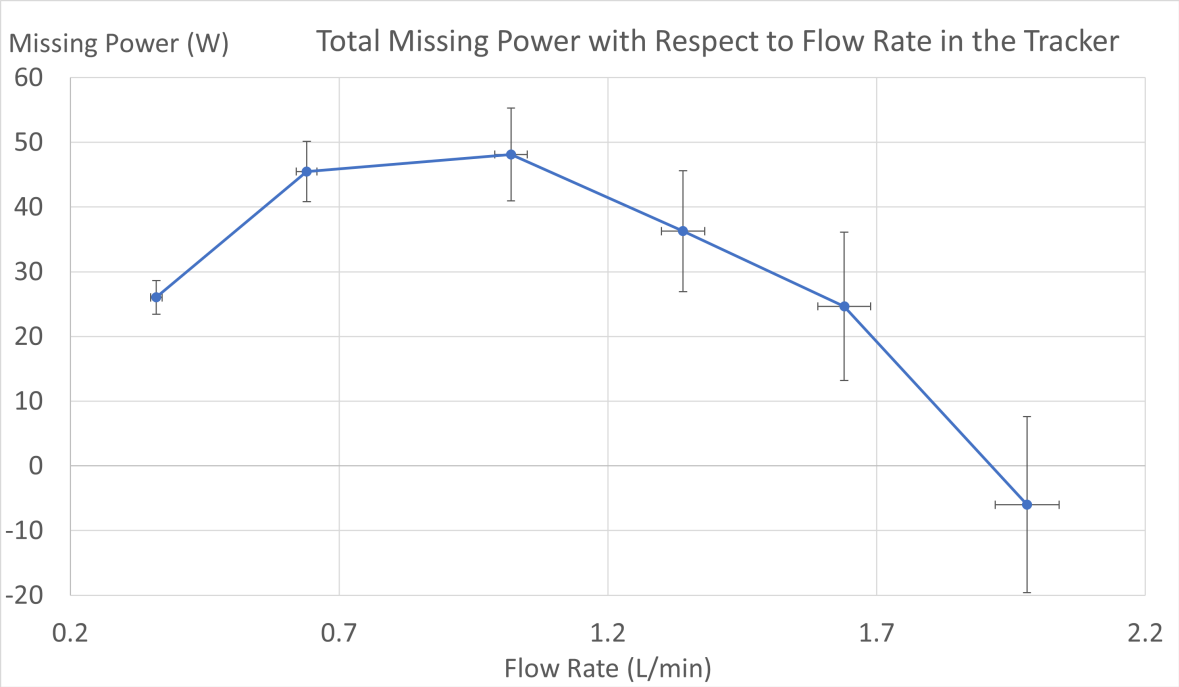

Figure 39: Missing power with respect to flow rate in the tracker. Notice the strange distribution which can be correlated with the type of flow present.

The graph for missing power tells a similar story to the one presenting energy absorbed by water in figure 38, showing of where different flow types were. However,

for almost all flows the unaccounted missing energy is comparable or larger than the energy put into the system. Uncertainty caused by PT-1000 and flowmeter error can't account for all of that missing energy, there is clearly something else at play, either some badness in measurement setup or wrong assumptions or just some property which isn't properly taken into consideration. Quite likely convection playing larger role than anticipated, or change of flow type to laminar. Similar thing is happening for low flow rates in the calorimeter, explained in chapter 8.2. With the current data, and methodology used in this thesis, it is not possible to determine what exactly went wrong. Characterizing why this is happening would require a more in-depth look at the energies in the tracker, for example by isolating the tracker. However, it's likely to provide too little useful information for the final prototype at this point in time.

8.1.2 Expected Cooling Performance

The results from various tests done on the tracker show quite conclusively that it will stay within temperature limits of the ALPIDEs. There is a lot of leeway in the amount of air and water flow, and the system can keep good temperatures with either or both. Of note is that the final design will be a slightly lighter, but it is expected to behave very similarly to the mock-up, with similar thermal stabilization time.

8.2 Calorimeter Results Discussion

The calorimeter was a surprise on some fronts. The general temperature measurement spots were not too obvious, therefore many auxiliary spots were chosen, as per chapter 5.5. The air temperatures without air escaping were at points higher than the 40 °C limit we would like to stay below, however this is an extreme case. The absorber layer temperatures, which were only regulated by free convection, looked very good, see table 12 and figure 13. As well as that the temperature drop across the plate was very good at 2.9 °C, compared to the expected 1.7 °C calculated in 3.6:

Table 12: Temperatures at the absorber plates in the calorimeter. W.Arrow means White Arrow and together with Red Arrow are the spots visible in figure 13

Spot	**W.Arrow: 1**	**W.Arrow: 2**	**W.Arrow: 3**	**Red Arrow**
Temperature	39.1±0.1 °C	36.2±0.1 °C	38.5±0.1 °C	Chassis Temperature, not interesting

The general behavior of the system with changing power levels and constant coolant flow is linear, this was within expectations as the calorimeter is massive and barely affected by sudden changes in environment.

The results for air temperature inside the calorimeter were linear, as expected. Looking at them it is easy to conclude that reducing the water temperature would be a quick solution for keeping ALPIDE cold enough. However, the condensation of water vapor must be considered carefully, as any condensation would have really bad consequences for the ALPIDE sensors inside. So, even though no condensation was observed for any of the setpoint temperatures tested, the same can't be guaranteed for all times of the year and weather types. For safety, the setpoint should stay above 16 °C, and ideally remaining at the default 18 °C.

8.2.1 Heat Removed by Water in the Calorimeter

From results in figure 35, it is possible to calculate the heat absorbed by water, with values and uncertainties visible in table 13 and plotted on figure 41. As mentioned in chapter 3.9, the flow is assumed to split between the two cold plates evenly, as they are in parallel. So the Flow rate through each plate in table 13 is the total flow rate divided by two, as there are two cold plates.

Table 13: Calculated heat absorbed by water with uncertainties.

Flow rate (L/min)	**Average ΔT over 2 chilling cycles in top cooling plate (°C)**	**Average ΔT over 2 chilling cycles in bottom cooling plate (°C)**	**Energy absorbed, top cooling plate (W)**	**Energy absorbed, bottom cooling plate (W)**
11.8±0.35	1.04±0.14	0.93±0.14	433.28±60.10	386.15±59.81
10.8±0.32	1.11±0.14	0.98±0.14	416.59±54.70	369.92±54.40
9.37±0.28	1.36±0.14	1.20±0.14	443.89±48.08	391.59±47.67
7.96±0.24	1.64±0.14	1.45±0.14	455.26±41.56	401.90±41.06
6.00±0.18	2.34±0.14	2.01±0.14	489.91±33.03	421.24±32.17
4.33±0.13	3.73±0.14	3.17±0.14	563.27±27.23	478.16±25.72
3.38±0.10	5.91±0.14	5.02±0.14	697.02±26.74	591.74±24.35

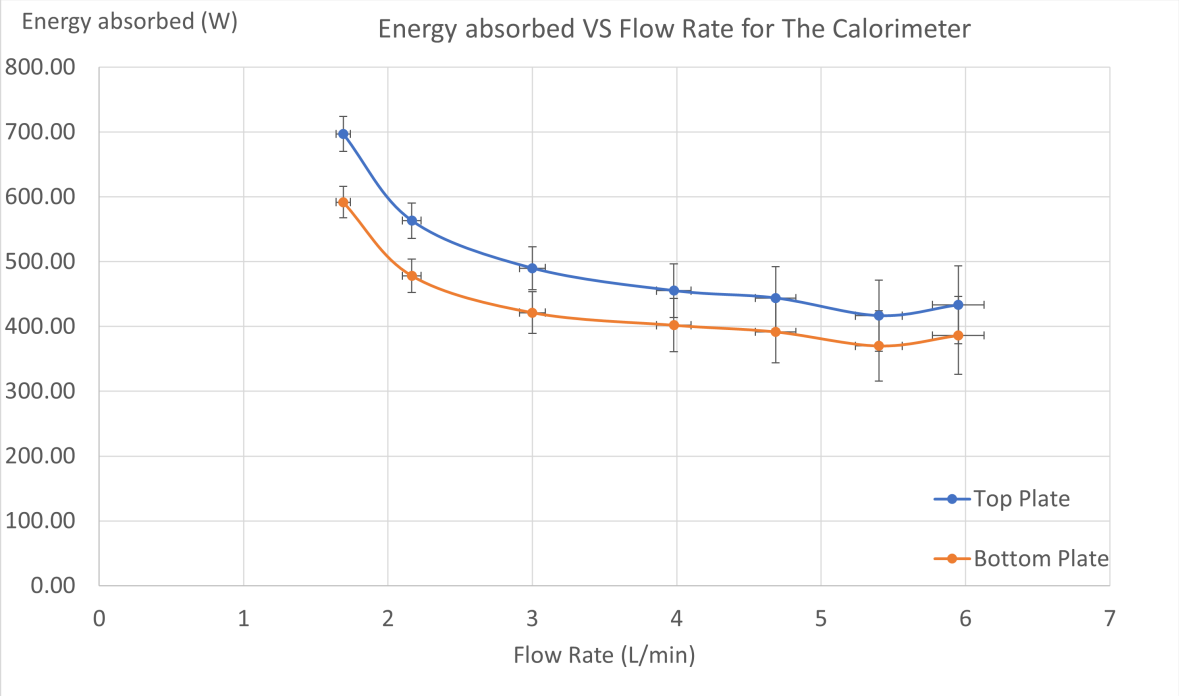

Figure 40: Heat absorbed by water in top and bottom cooling plate in the calorimeter.

Figure 40 shows how much energy was absorbed by water in the top and bottom cooling plates in the calorimeter. The flow type is expected to be turbulent for all

values, as also seen in table 14 below. However, values of Reynold's number for low flow rates lie in the transitional range which could be part of the reason for the rise in energy absorbed.

Table 14: Flow rate through each plate in the calorimeter and its corresponding Reynold's number

Flow rate (L/min)	1.69	2.17	3.00	3.98	4.69	5.40	5.90
Reynold's number	2978	3824	5287	7014	8266	9517	10398

These values can then be used to calculate the total energy in table 15.

Table 15: Calculated total power in the system, as given in chapter 3. Q_L is the sum energy absorbed by water in top and bottom cooling plate in the calorimeter, with values found in table 12. Uncertainties of P_E, P_M, Q_C << uncertainty of Q_L, in the order of 1 to 100 and are therefore ignored for simplicity, see chapter 3.5.

Flow Rate (L/min)	Q_L**(W)**	P_E**(W)**	P_M**(W)**	Q_C**(W)**	**Missing Power (W)**
11.80	819.43±84.79	809.95	51.59	-11.30	-30.81±84.79
10.80	786.51±77.14	809.95	42.43	-10.12	-55.74±77.14
9.37	835.48±67.71	809.95	31.55	-8.37	2.36±67.71
7.98	857.16±58.42	809.95	23.00	-6.23	30.45±58.42
6.00	911.16±46.11	809.95	14.22	-0.58	87.57±46.11
4.33	1041.43±37.46	809.95	8.87	10.32	212.29±37.46
3.38	1288.76±36.17	809.95	6.46	24.92	447.43±36.17

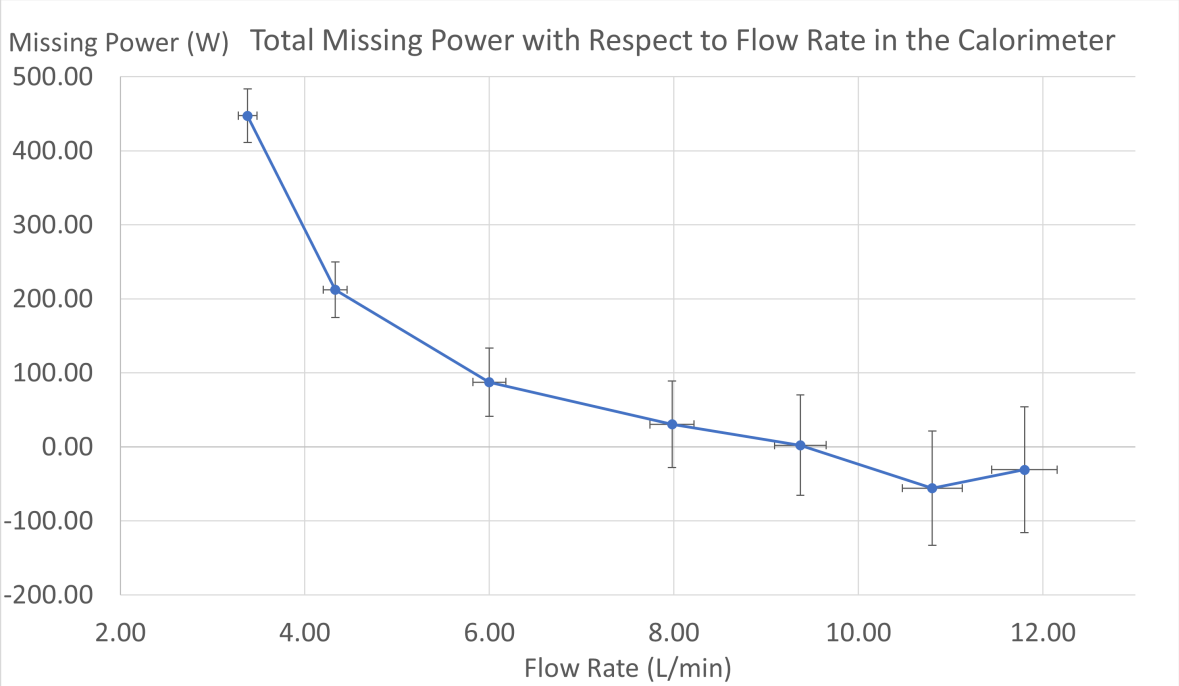

Figure 41: Missing power with respect to flow rate in the calorimeter. Notice the large amounts of energy missing at low flow rates.

At high flow rates, the missing power is relatively small and could be explained by simple inaccuracies in measurements and limitations imposed by assumptions made. For example, measurements in temperature of water are less accurate than desired. On the other hand, behavior at lower flow rates diverges so greatly that it no longer lies within any error margins. This behaviour sort of mimics the one for the tracker, which could indicate some systematic error at lower flow rates, perhaps caused by laminar flow. This would require further investigation. However, the system is not expected to run at low flow rates and characterizing energy removed by coolant in this range may simply not be desirable.

8.2.2 Expected Cooling Performance of the Finished Prototype

The results from various tests done on the calorimeter above help draft a conclusion on its expected performance. While the calorimeter mock-up just barely misses the ALPIDE temperature requirements in some specific cases, the final prototype is expected to perform within temperature limits of the ALPIDEs at its maximum cooling output, while still allowing a sizeable margin in reduction of this output without increas-

ing temperatures dramatically. The reason for this conclusion lies largely in difference in heat distribution between the mock-up and final prototype. Most of the measurements were done in areas close to or directly affected by the heat sources, meaning the heat was higher than it would be otherwise. In the final prototype the heat sources will be evenly distribution in the whole volume, and not along top and bottom of of it.

8.3 Expected Thermal Stabilization Time of the Finished Prototype

Given the results in 7.1 and the simple model found in 3.1, it can be safely predicted that the final prototype of the calorimeter will take around 7-8 hr and the tracker to take around 15 min to fully thermally stabilize. The result for the calorimeter is strong, as the extra mass that will be there in the final prototype will be in the center of it, so the total area from which energy can escape doesn't really increase. The result for the tracker is strong, as the total mass isn't expected to change by any significant amount.

The critical performance point of the DTC is of little interest, as the machine is never intended to run below 50% of performance. As well as that, there is no possiblity of measuring for flow rates below the ones the flowmeters are able to measure, meaning this point might not even be currently measurable. However, for the calorimeter in figure 33, we can see a clear change in temperature increase rates for flow rates below 3.5 L/min or roughly 30% performance. The tracker is expected to just increase in temperatures mostly linearly with reduced cooling performance as temperature, as both 26 and 32 show nearly linear increase as well.

8.4 On Ambient Temperature Increase

During testing, the issue of lab temperature increase was mostly omitted. Naturally, the air temperature will increase due to heat from the DTC, this is not noticeable when heating the tracker layer but rears its head whenever the calorimeter heating is at high power for a long period of time, in hours.

It was observed that increases in ambient temperatures correlate quite linearly to increases in temperature at various parts of the DTC, almost 1:1 at the temperatures

the DTC was operated. However, measuring this effect was not possible in the current environment, due to lack of ambient temperature control and the chiller operating in the same room. This effect was observed to go both ways, so increasing ambient temperatures and reducing ambient temperatures is expected to respectively increase and reduce temperatures at the DTC. Studying this could potentially be beneficial in characterising the prototype.

8.5 On Flow Rate Divergence from Expected Values

One of the first parts of working with this thesis was to find out how the system currently performs and trying to optimize it with regard to all three valves on the machine, in order to achieve values from chapter 4.4. The final values for flowrate achieved can be found in chapter 4.5, and they agree within 19% for the tracker, and 12% for the calorimeter. This was a concern at first, but after testing the water cooling, the cooling performance barely changes when reducing flow rate down to about 80% of maximum value.

8.6 On Long Term Performance of the DTC

During testing, the DTC was usually running between 6-8 hr non-stop. Although no hardware issues were observed and the performance was stable without any sudden changes, one important issue on the software-end came up. Currently the Moxa I/Os are connected to the university network, so they are easily available from any computer connected to it. However, this creates a problem as the university network at times shuffles IP addresses of the Moxa I/Os, resulting in loss of connection and thus readout. Circumventing the issue was quite quick with experience, however, until the setup is moved to its own local network, anyone working with it should be made aware of this fact.

8.7 Outlook

This work ended up finding a few interesting and useful properties of the DTC prototype mock-up which can be translated into the final prototype. While the calorimeter

couldn't be emulated due to how different the mock-up is, the total energy supplied was similar and many thermal properties could be investigated. On the other hand, the tracker can be expected to behave similarly with C-E layers and ALPIDEs instead of aluminium and heating strips, so results could potentially be applied 1:1 from mock-up to final prototype.

We see well defined temperature trends, most of which are linear, for both the tracker and the calorimeter. Many of which will be useful for tweaking the more complete system. The investigation into how reduced water cooling performance affects temperatures will allow for sparing various mechanical parts of the water cooling, as running everything at 100% is not optimal from performance and durability stand point.

The thermal stabilization time measurement for current mock-up and the prediction of that value for the final prototype based on that measurement are both very important results, when keeping in mind that ALPIDE sensors get more noisy the hotter they are.

The results for power removed by water cooling, while lackluster for the tracker and at calorimeter low flow rates and with large uncertainties, still provide a good estimate of how much energy can be expected to dissipate into the environment instead of water. However, they would need to be redone with more accurate measurements if the need arises.

Additionally, there are a couple recommendations for those working with the DTC cooling system in the future:

- Even though it is not an issue at this point, the slow formation of residue in the water cooling loop should be looked at least every year. It is both a inhibitor of heat conduction and water flow, and will, given enough of it, negatively affect the chiller pump and chiller itself.

- It is recommended to develop a method for fine fan control and speed readout via MOXA E1212. While the fans can be activated and quite crudely controlled via any MODBUS script at this point in time, they were only used a few times. When they were, they were left running at maximum output, which generates a constant, loud and unpleasant noise.

Appendix A - Readout and Software Details

Raw data coming from all the sensors needs to be processed before being displayed. The steps required are described in this chapter. This includes a description of how Moxa I/Os read data from sensors and process.

Moxa E1240

For the Moxa E1240, the analog data collection happens in the following steps:

1. Analog signal is received, either a voltage or current depending on what type of sensor we are interested in reading.

2. Data is digitized, and depending on its value, assigned linearly to a number from 0 to 65535, a 16-bit size data piece. Example: 0V/4mA would be integer 0 and 10V/20mA would be integer 65535. Giving a good resolution

3. Data is then either pushed to the web server the module is running or through an IP connection to any client desired using MODBUS protocol.

Moxa E1260

Although analog, this unit doesn't output data in the same way as the Moxa E1240. With this unit, no way of reading out a digitized value of current signal was found. Instead it always outputs a temperature reading based on resistance in RTD sensors, with pre-made scaling options for different types sensors, for example PT-100 or PT-1000. In practice, this means we have temperature reading resolution limit of 0.1 °C as set by the unit manufacturer.

Moxa E1212

Moxa E1212 is unique in the fact that input and output signals are digital, so there are no complications with sending and receiving data. This unit saw rare use and its details weren't investigated as it was deemed irrelevant for contents of this thesis. However, there is some strangeness with reading fan speeds, identified for now to be

the configurable digital filter. This would require further investigation for proper fan speed readout.

Required Library

Currently, other than python itself, a single extra library is required, PYMODBUS [24]. PYMODBUS itself doesn't have any third party dependancies. Many good examples of how this library can be used are found on their website

Appendix B - Starting the Mock-up and Detector Cooling System

Starting the Mock-up

To start the mock-up, first plug in the chiller, and the power supplies for the tracker and calorimeter into the power outlets. Starting with the chiller, make sure the chiller valve is closed before starting it, this prevents sudden spikes in pressure which could damage the pressure transducers. After the pump starts running, open the valve. The power to heating elements can be controlled by via power supplies.

Starting the Cooling System Hardware

Starting the cooling system is done by connecting it to a power outlet and turning on the left-most switch, the other switch turns off/on the fans.

Starting the DCS Software

Here starting up all the necessary software for readout, database and display is described. In no particular order:

- Readout software is written in python, located at Bergen pCT Github. Started using a command in windows terminal (cmd): *py CoolingMonitoring_api_allMoxa.py*

- Database software is located locally at the UiB. First open a Windows Powershell terminal, then go to location of influxDB.exe or by command *cd ´\Program Files\InfluxData\influxdb\influxdb2_windows_amd64´* and start it using ./influxdb.exe
- Accessing the database is done through any web browser. InfluxDB is available at **localhost:8086** requiring no credentials. Grafana is available at **localhost:3000**, default username: *admin*, default password: *admin*. Just type them into the search/url bar.

Bibliography

References

[1] L. Whitmore, R. I. Mackay, M. Van Herk, J. Jones, and R. Jones, "Focused vhee (very high energy electron) beams and dose delivery for radiotherapy applications," *Scientific Reports*, vol. 11, no. 1, pp. 1–14, 2021.

[2] J. Alme, G. G. Barnaföldi, R. Barthel, V. Borshchov, T. Bodova, A. Van den Brink, S. Brons, M. Chaar, V. Eikeland, G. Feofilov, *et al.*, "A high-granularity digital tracking calorimeter optimized for proton ct," *Frontiers in Physics*, vol. 8, p. 568243, 2020.

[3] Utrecht University, Anthony van den Brink. Private communication.

[4] J. M. Kocarnik, K. Compton, F. E. Dean, W. Fu, B. L. Gaw, J. D. Harvey, H. J. Henrikson, D. Lu, A. Pennini, R. Xu, *et al.*, "Cancer incidence, mortality, years of life lost, years lived with disability, and disability-adjusted life years for 29 cancer groups from 2010 to 2019: a systematic analysis for the global burden of disease study 2019," *JAMA oncology*, vol. 8, no. 3, pp. 420–444, 2022.

[5] Helse og Omsorgsdepartementet, "Etablering av Protonsentre I Bergen og Oslo, [Establishment of Proton Centers in Bergen and Oslo]," https://www.regjeringen.no/no/dokumentarkiv/regjeringen-solberg/aktuelt-regjeringen-solberg/hod/pressemeldinger/2017pm/etablering-av-protonsentre-i-bergen-og-oslo/id2579970/, Last Accessed 12.05.2023.

[6] M. Aehle, J. Alme, G. Barnaföldi, T. Bodova, V. Borshchov, A. van den Brink, M. Chaar, V. Eikeland, G. Feofilov, C. Garth, *et al.*, "The bergen proton ct system," *Journal of Instrumentation*, vol. 18, no. 02, p. C02051, 2023.

[7] C. Borek, "Antioxidants and radiation therapy," *The Journal of nutrition*, vol. 134, no. 11, pp. 3207S–3209S, 2004.

[8] J. M. Brown, "Tumor hypoxia in cancer therapy," *Methods in enzymology*, vol. 435, pp. 295–321, 2007.

[9] M. J. Gazda and L. R. Coia, "Principles of radiation therapy," *Cancer management: a multidisciplinary approach*, 2001.

[10] R. Mohan and D. Grosshans, "Proton therapy–present and future," *Advanced drug delivery reviews*, vol. 109, pp. 26–44, 2017.

[11] T. Bortfeld, "An analytical approximation of the bragg curve for therapeutic proton beams," *Medical physics*, vol. 24, no. 12, pp. 2024–2033, 1997.

[12] N. Krah, D. Dauvergne, J. M. Létang, S. Rit, and E. Testa, "Relative stopping power resolution in time-of-flight proton ct," *Physics in Medicine & Biology*, vol. 67, no. 16, p. 165004, 2022.

[13] R. Kataura, T. Izumikawa, T. Konno, and T. Kawasaki, "Stopping power measurement for proton therapy by combining proton radiography and x-ray ct," *Nuclear Instruments and Methods in Physics Research Section A: Accelerators, Spectrometers, Detectors and Associated Equipment*, vol. 1027, p. 166316, 2022.

[14] M. Mager, A. collaboration, *et al.*, "Alpide, the monolithic active pixel sensor for the alice its upgrade," *Nuclear Instruments and Methods in Physics Research Section A: Accelerators, Spectrometers, Detectors and Associated Equipment*, vol. 824, pp. 434–438, 2016.

[15] W. Poonsawat, C. Kobdaj, M. Sitta, and Y. Yan, "Stave module design and development of the new alice inner tracking system," *Journal of Instrumentation*, vol. 14, no. 05, p. P05003, 2019.

[16] V. Zherebchevsky, I. Altsybeev, G. Feofilov, A. Francescon, C. Gargiulo, S. Igolkin, E. Krymov, E. Laudi, T. Lazareva, N. Maltsev, *et al.*, "Experimental investigation of new ultra-lightweight support and cooling structures for the new inner tracking system of the alice detector," *Journal of Instrumentation*, vol. 13, no. 08, p. T08003, 2018.

[17] C. Bopp, R. Rescigno, M. Rousseau, and D. Brasse, "The impact of tracking system properties on the most likely path estimation in proton ct," *Physics in Medicine & Biology*, vol. 59, no. 23, p. N197, 2014.

[18] Á. Sudár, "Measurement of the temperature distribution inside a calorimeter," *arXiv preprint arXiv:2005.02830*, 2020.

[19] F. M. Widerøe, "Mechanical design and thermal properties of the carbon layers of the proton ct tracking system," Master's thesis, The University of Bergen, 2021.

[20] https://www.moxa.com/en/products/industrial-edge-connectivity/controllers-and-ios/universal-controllers-and-i-os/iologik-e1200-series, Last Accessed 24.05.2023.

[21] University of Bergen, Håvard Birkenes. Private communication.

[22] https://www.smcpneumatics.com/pdfs/PF3W.pdf, Last Accessed 25.05.2023.

[23] https://www.lauda.de/pimimport/assets/context/pdmarticle/13/1307/13077/attachments/Export.13077.2018-10-12-09-04-55.713056d3.pdf, Last accessed 01.06.2023.

[24] https://pypi.org/project/pymodbus/, Last Accesed 26.05.2023.